Altermagnetism: A Chemical Perspective

Shannon S. Fender,[†,¶] Oscar Gonzalez,[†,¶] and D. Kwabena Bediako[*,†,‡]

†*Department of Chemistry, University of California, Berkeley, California 97420, United States*

‡*Chemical Sciences Division, Lawrence Berkeley National Laboratory, Berkeley, California 94720, United States*

¶*Contributed equally to this work*

E-mail: bediako@berkeley.edu

Abstract

Altermagnets have been recently introduced as a classification of collinear, spin compensated magnetic materials that host net-zero magnetization, yet display some electronic behaviors typically associated with non-compensated magnetic materials like ferromagnets. The emergence of such properties are a consequence of spin-split bands that arise under specific symmetry conditions in the limit of zero spin–orbit coupling. In this Perspective, we summarize the fundamental criteria for realizing an altermagnetic phase and present a qualitative electronic band structure derivation and symmetry analysis through chemical principles. We then discuss the properties that make altermagnets distinctive candidates for charge-to-spin conversion elements in spintronic devices, and provide a brief review of some altermagnetic candidate materials. Finally, we discuss future directions for altermagnetism and highlight opportunities for chemists to advance this emerging field.

Introduction

As silicon-based semiconductor technologies approach their performance limits amidst rising demands for faster, denser, and more powerful computing, device architectures that leverage many-body electronic and magnetic interactions have been proposed as a means to advance beyond Moore's Law.[1] "Spintronics" is the general term for computing and/or memory schemes that leverage the electronic spin degree of freedom to encode, store, and manipulate information through phenomena that include long-range[2] or local magnetic order[3] and spin-waves/magnons.[4] Traditional spintronic devices are based on ferromagnets, as magnetization serves as a straightforward means of encoding and reading out information.[2] However, memory devices based on ferromagnetic materials are inherently limited since their stray fields can lead to data instability at high storage densities as well as lower data security. Instead, contemporary interest in spintronics has shifted to materials with compensated magnetic moments, like antiferromagnets.[5–10] The incorporation of spin-compensated magnetic materials into spintronic frameworks provides key advantages, including faster switching dynamics, greater insensitivity to destabilizing fields (leading to higher integration density and improved data security), as well as reduced power consumption and improved overall efficiency.[6] A major focus of this field is understanding and exploiting antiferromagnetic materials that can host phenomena like giant magnetoresistance, the anomalous Hall effect, and spin-transfer-torque, which underpin more conventional ferromagnetic spintronics.[6]

Recently, theoretical predictions and experimental observations have identified a subset of spin-compensated magnetic materials that exhibit large anomalous Hall effects and spin-split electronic band structures that are typically associated with non-compensated magnetic materials like ferromagnets.[11–15] It is worth noting that this general phenomenology had been identified almost three decades ago by Solovyev in perovskites, and by others later, but has received intense interest in recent years.[16–19] The term "altermagnetism" has since been coined as a classification for these materials in which alternating local coordination environments around metals associated with opposite spin sublattices result in spin-split

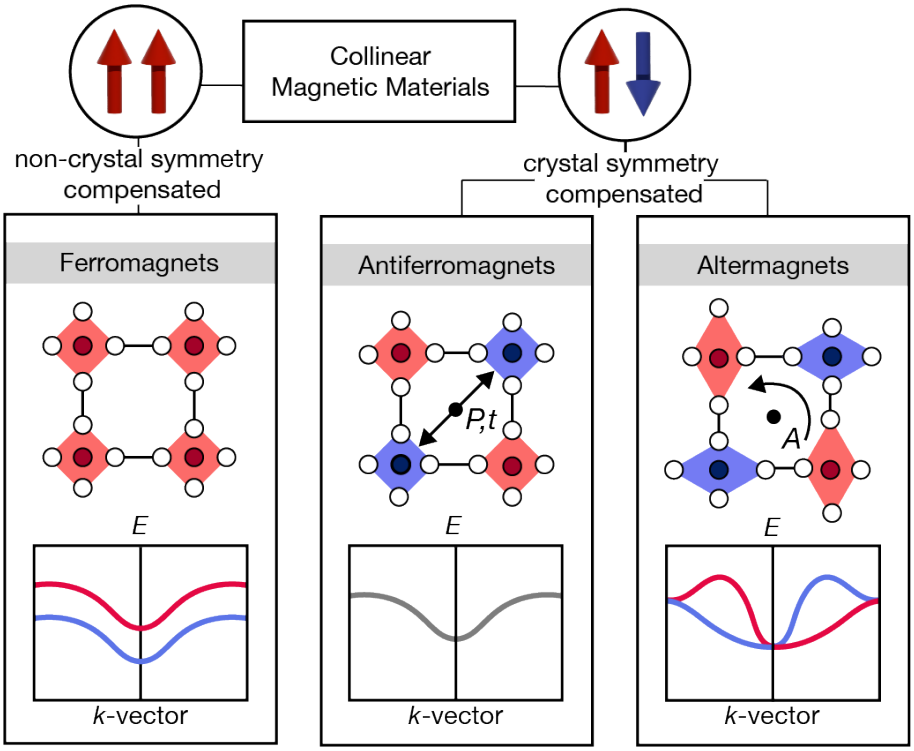

Figure 1: Three types of collinear magnetic materials that can be described by nonrelativistic spin group conventions. P, t, and A refer to inversion, translation, and rotation symmetry operations, respectively.

bands. It is this phenomenon that allows the electronic properties typically associated with net spin polarization to emerge in materials with vanishingly small magnetization.[13]

The key structural feature of altermagnetic materials is the presence of crystallographic rotation operations connecting opposite spin sublattices that cannot be transposed by inversion, translation, mirror reflections, or their combinations.[12,13] Theoretical treatments of altermagnetism use a nonrelativistic spin group convention to delineate collinear magnets into the three magnetic classes outlined in Figure 1. In this classification, transformations, R, are described by $[\mathrm{R}_i||\mathrm{R}_j]$, where $[\mathrm{R}_i|$ operates solely on the magnetic moment vectors in spin space and $|\mathrm{R}_j]$ acts on the atoms in real space.[13] This differs from the conventional framework used to describe magnetic crystal symmetry, which involves transformations that simultaneously act on both the atoms and magnetic moment vectors of the crystal lattice,[13] leading to classification via magnetic space groups. Classifications using magnetic space

groups, described in 1984 by Landau and Lifshitz, link magnetic properties to the symmetry of electronic motion through an orbital-current model of magnetism.[20] As a result, coupling real and spin space symmetries via magnetic space groups is a fundamentally relativistic exercise. Using nonrelativistic spin groups effectively decouples spin and orbital moments, uncovering an altermagnetic parent phase with spin-split bands that are otherwise hidden through a relativistic analysis. Altermagnetic spin splitting thus arises without spin-orbit coupling and is instead entirely due to real and spin space symmetries, making it feasible in materials containing light elements.

Altermagnetism is specifically characterized by the interplay of two rotations: a C_2 rotation that maps collinear spin-up and spin-down magnetic moments onto each other, combined with any rotation operator, A, that acts only on the real space lattices associated with each spin center. Notably, the rotation operator A can be proper or improper and symmorphic or nonsymmorphic, often taking on the form $A = [C_n t]$.[13] Denoted together as $[C_2||A]$, this symmetry is distinct from other collinear magnetic classes (ferromagnetism and "conventional" antiferromagnetism) because it connects real-space opposite spin sublattices through rotation, rather than via space inversion or translation. To understand how rotation symmetries give rise to altermagnetic spin-splitting, it is useful to consider a conventional antiferromagnet, where the real-space sublattices are interconvertible by P. In an antiferromagnet, compensated spins combined with translation or inversion operators ($[C_2||t]$ and $[C_2||P]$ respectively) will lead to the uniform evolution of spin-up and spin-down bands through momentum space, which restores the macroscopic spin degeneracy in the overall band structure. In an altermagnet, the real-space rotational symmetry connecting the sublattices induces a momentum-space mismatch in the dispersion of spin-up and spin-down bands. Spin splitting thus arises in localized regions of the electronic structure where spin degeneracy is not restored, and the emergence of this spin splitting is closely tied to the rotated real-space environments that preclude P. As a result, compensated spins in an altermagnet can give rise to phenomena associated with broken time-reversal symmetry, ($\mathcal{T}$).[13]

This alternating spin polarization in both real space and in the resulting momentum-space electronic environment is also the origin of the coined name "altermagnetism".[12]

The symmetry framework described above effectively defines non-relativistic spin splitting (NRSS) phenomena in collinear, spin-compensated materials. However, NRSS effects are also reported in materials that lie outside the scope of altermagnetism, such as noncollinear antiferromagnets.[21] Therefore, there exists an alternative perspective to view altermagnetism simply under the umbrella of unconventional AFMs.[22] While altermagnetism is not the only pathway to realizing NRSS phenomena in spin-compensated materials, given the broad applicability of the classification to collinear systems, it is a useful guideline for materials research.

Our focus in this Perspective is to first explain the emergence of non-relativistic spin splitting in altermagnets on the basis of chemical principles and symmetry, describe some of the most relevant electronic/spintronic properties of these materials, and then discuss examples of candidate altermagnet materials with a synopsis of recent experimental work on these systems. In doing so, we aim to re-frame these concepts from and for the chemist's point of view. While at least 50 compounds have already been predicted to be altermagnetic, few have been experimentally confirmed. The work of solid-state and synthetic chemists in new materials discovery coupled with experimental confirmation will expand the library of altermagnets and unveil novel phenomena and new frontiers, such as unconventional *d*-wave or higher even-parity order magnetism, unconventional topological superconductivity, dissipationless Hall transport, and new ways to design ultra-efficient charge-to-spin conversion in compact spintronic devices.[12,14]

The electronic band structure of altermagnets

The approach of predicting the band structures of extended solids through chemical principles, as popularized by Roald Hoffmann, underscores the connection between chemical intu-

ition and physical properties. This perspective combines Bloch's theorem and a molecular orbital description of chemical bonding to enable a first order "pen and paper" determination of a crystal's band structure.[23] As chemists, this view on the tight-binding model provides us with clear insight into the relevant molecular symmetries underlying solid-state band theory. Accordingly, it has been successfully applied to describe a variety of emergent phenomena, including the topology of square net lattices,[24,25] semiconductor band gaps of halide perovskites,[26] non-trivial surface bands in topological insulators,[27] and the linear dispersion of two-dimensonal (2D) Dirac semimetals.[28] Here, we use this approach to understand non-relativistic spin splitting in altermagnets.

Altermagnetism's core features and properties emerge from the spin-splitting of electronic energy bands in a material's momentum-space band structure, creating a region where time-reversal symmetry is broken. This spin-splitting is driven by the anisotropy in electronic band dispersion of spin-up and spin-down sublattices (as defined by the associated real-space bonding environments), which will transform under proper rotations closely tied to the overall symmetry of the resultant spin-splitting.[13,29–31] This effect, governed by the global lattice symmetries of the material, can be well-captured by Bloch's theorem.[32] Theoretical calculations have proposed several altermagnetic candidates, including the rutile structures RuO_2, MnO_2, and MnF_2.[12,15,33,34] While the magnetic ground state of RuO_2 remains a subject of intense debate (as discussed in later sections), for the purpose of a toy model, the rutile structure type serves as a useful and relatively simple starting point for us to demonstrate the connection between local chemical structure, rotational symmetry operations, and subsequent altermagnetic band splitting through a Hoffmann-like approach.

A portion of the rutile structure is depicted in Figure 2a. In this tetragonal structure type, metal centers are located in distorted octahedral geometries with inequivalent axial and equatorial bond lengths. Along the *c*-axis, octahedra are edge-sharing, whereas in the *ab* plane, octahedra are corner-sharing across the shorter, axial bonds. The axial directions of the octahedral environment are uniformly aligned within a layer of the *ab* plane and

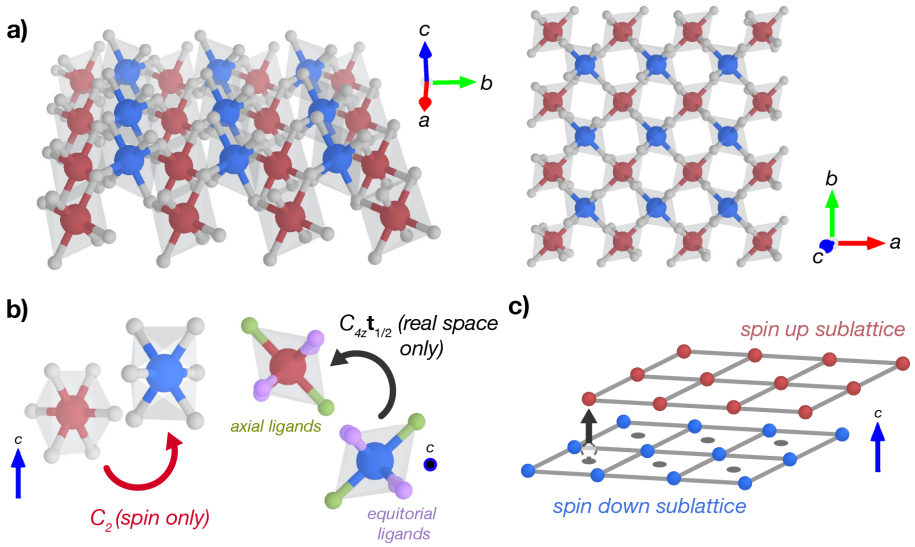

Figure 2: Crystallographic and magnetic representation of a simple altermagnetic rutile. a) Lateral expansion of the simple rutile unit cell shows rotated octahedral environments for spin-up and spin down lattices, which are represented by red and blue metal centers respectively. b) Spin-space C_2 and real space $C_{4z}\mathbf{t}_{1/2}$ transformations link opposite spin sublattices by rotation symmetries, leading to altermagnetism. c) Segregating spin-up and spin-down lattices onto two offset ferromagnetic square nets will also give rise to altermagnetic band splitting.

transform by a 90° rotation respective to their c-axis nearest neighbors. The local distortion to the coordination environment in rutile structures is attributed to the packing arrangement of atoms, and the relative degree of the distortion depends on the relative sizes of the cation and anion as observed in TiO_2, VO_2, CrO_2, and ZnF_2.[35] Geometric distortions to the local coordination environment can also be electronically driven by the Jahn–Teller effect.[36] For an altermagnetic rutile, the spin structure necessarily adopts a collinear, A-type compensated spin pairing,[12,29,30] which is shown in Figure 2a by the depiction of spin up (red) and spin down (blue) polyhedra occupying alternate layers in the form of edge-sharing chains.

In rutile structures, the real-space symmetry of a distorted octahedral coordination environment is imposed on the local electron and spin density of each metal center. The electron density of spin up and spin down octahedral sites transform according to $C_{4z}\mathbf{t}_{1/2}$ symmetry operation,[12,13,29] which corresponds to a real-space C_4 rotation around the c-axis accompanied by a half-magnetic unit cell translation. When a collinear, compensated spin orientation

is considered independent of the real-space environment, the spin symmetries transform by a C_2 rotation.

To illustrate how momentum-dependent spin splitting arises from these simple symmetry considerations, we use a toy rutile-like model consisting of rotated octahedra within an isolated bilayer. Spin polarization is enforced for all octahedra within each ab plane, thus, spin up and spin down metal centers of the lattice can be segregated onto independent 2D square lattices as depicted in Figure 2c. With this approach, we can analyze the dispersion of each spin sublattice at different points in momentum space.

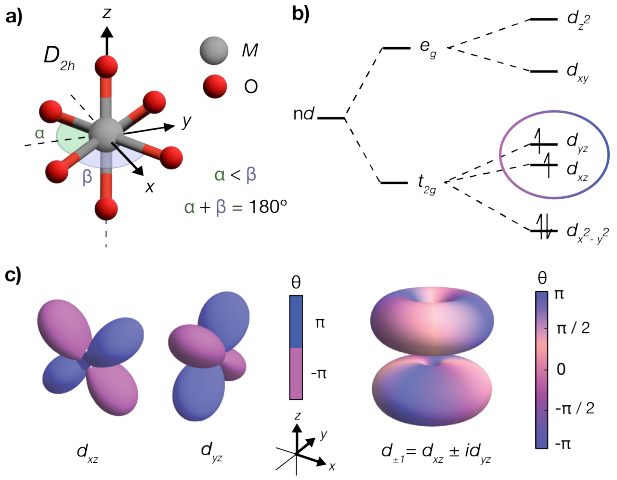

Figure 3: Crystal field splitting and Fermi-level bands of the rutile toy model. a) Distorted octahedral environment surrounding spin-bearing metal centers, denoted as M. Axial bonds along the z axis are shorter than the equatorial bonds along the xy plane. b) Molecular orbital diagram highlights the highest occupied orbitals after distortion from an octahedral crystal field environment using a d^4 metal cation. c) Complex linear combination of frontier atomic orbitals d_{xz} and d_{yz}. Orbital phase is denoted by θ and the resulting sign for the real-space orbitals is determined by $\cos(\theta)$.

The next consideration lies in the choice of orbitals. In the band structure of rutile MO_2 (where M^{2+} is a d^4 metal cation), simple ligand-field theoretical calculations indicate that the frontier d orbitals responsible for the bands that cross the Fermi-level are a linear combination of d_{xz} and d_{yz} orbitals (this is also anticipated from a simple d-orbital splitting analysis of the MO_6 octahedra), as shown in Figure 3.[37,38] It is important to note, however, that spin splitting will occur for any metal d orbital aligned to the local coordination axis; the spin

splitting in momentum space is the result of global symmetry operations and is not restricted to specific orbitals. Thus, the "altermagnetic" splitting will arise in all d-orbital-based bands. For simplicity, we consider a single d_{z^2} orbital on metal centers, oriented along the local axial direction of the spin centers. Because d_{z^2} orbitals transform with the same symmetry as the calculated real-space spin density of proposed altermagnetic rutiles,[12,13,23,25,26] we establish a correspondence between the spin-splitting derived in this simple model and the anticipated spin-splitting near the Fermi level of related materials.

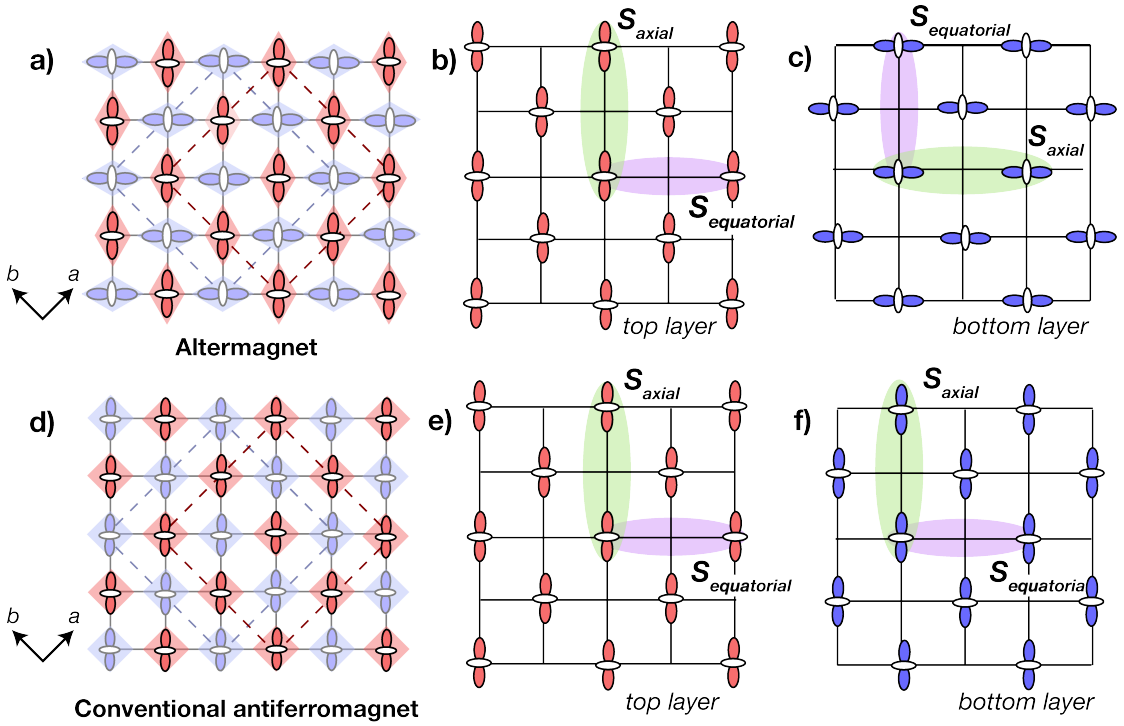

Figure 4: Coordinate systems for the altermagnetic (a-c) and antiferromagnetic (d-f) toy models. a) In the altermagnetic model, the local geometry around the spin-bearing centers dictates the orientation of d orbitals. The relative orientation remains consistent across a given sublattice, with a rotation transformation transposing spin–up (red) and spin–down (blue). The red and blue dashed lines represent the independent treatment of each sublattice, as shown in b-c). b) For the spin-up sublattice, interaction energies are defined by S_{axial} and $S_{equatorial}$, with stronger interactions occurring along the S_{axial} direction via intervening ligands (not shown). c) In the spin-down sublattice, interaction energies switch along the same real-space path compared to the spin-up sublattice. d) In the antiferromagnetic toy model, interconvertible local structure geometries lead to uniform d orbital alignment. As a result, equivalent interaction energies characterize the dispersion in e) spin–up and f) spin–down sublattices along a given real-space path of the antiferromagnetic toy model.

Following this reasoning, we orient d_{z^2} orbitals along the direction established by the local coordination geometry of each spin sublattice for an altermagnetic rutile in Figure 4a. The relative magnitude of interactions along axial and equatorial directions can be estimated from some chemical intuition of their overlap energies. Here, S_{axial} is attributed to the stronger interaction energy along the axial direction of d_{z^2} orbitals, and $S_{equatorial}$ is attributed to comparatively weaker interaction along the equatorial direction. The sign that can be attributed to this energy overlap, negative or positive, will depend on bonding versus anti-bonding interactions respectively. For this coordinate system, the interactions of d_{z^2} orbitals with two neighboring metal orbitals along the axial direction, as opposed to the two orbitals along the equatorial direction, occur in opposite real- and reciprocal-space directions for each sublattice. Thus, due to the rotated orientation of the spin sublattices shown in Figures 4b and 4c, the relevant net interaction integral along a specific path through the real-space crystallographic lattice will switch for the opposite spin sublattice. In reality, there is no meaningful direct metal–metal orbital overlap, but these interactions and the spin sublattice-dependent band dispersions that result are instead mediated by the intervening ligands. Nevertheless, this model where we only depict the spin-bearing d-orbitals is a helpful start for understanding the local, orbital origins of spin splitting in altermagnets. In contrast, as shown in Figure 4d for the antiferromagnetic case (possessing the spin space C_2 symmetry, but lacking the orbital rotations due to real-space localized distortions), an isotropic ligand coordination leads to the identical alignment of d_{z^2} orbitals for both spin sublattices. As shown in Figure 4e and 4f, the dispersion for spin up and spin down orbitals of the antiferromagnet will therefore be equivalent along both crystallographic paths of the square lattice.

In Figure 5a, we establish a basis (outlined by a dashed grey line) for our isolated bilayer, which also corresponds to the basis of a generalized rutile unit cell. The first 2D Brillouin zone (BZ) of the toy model is shown in the lower right of Figure 5a, describing the high-symmetry points of the square lattice in momentum space, which we shall use in the treatment of the two

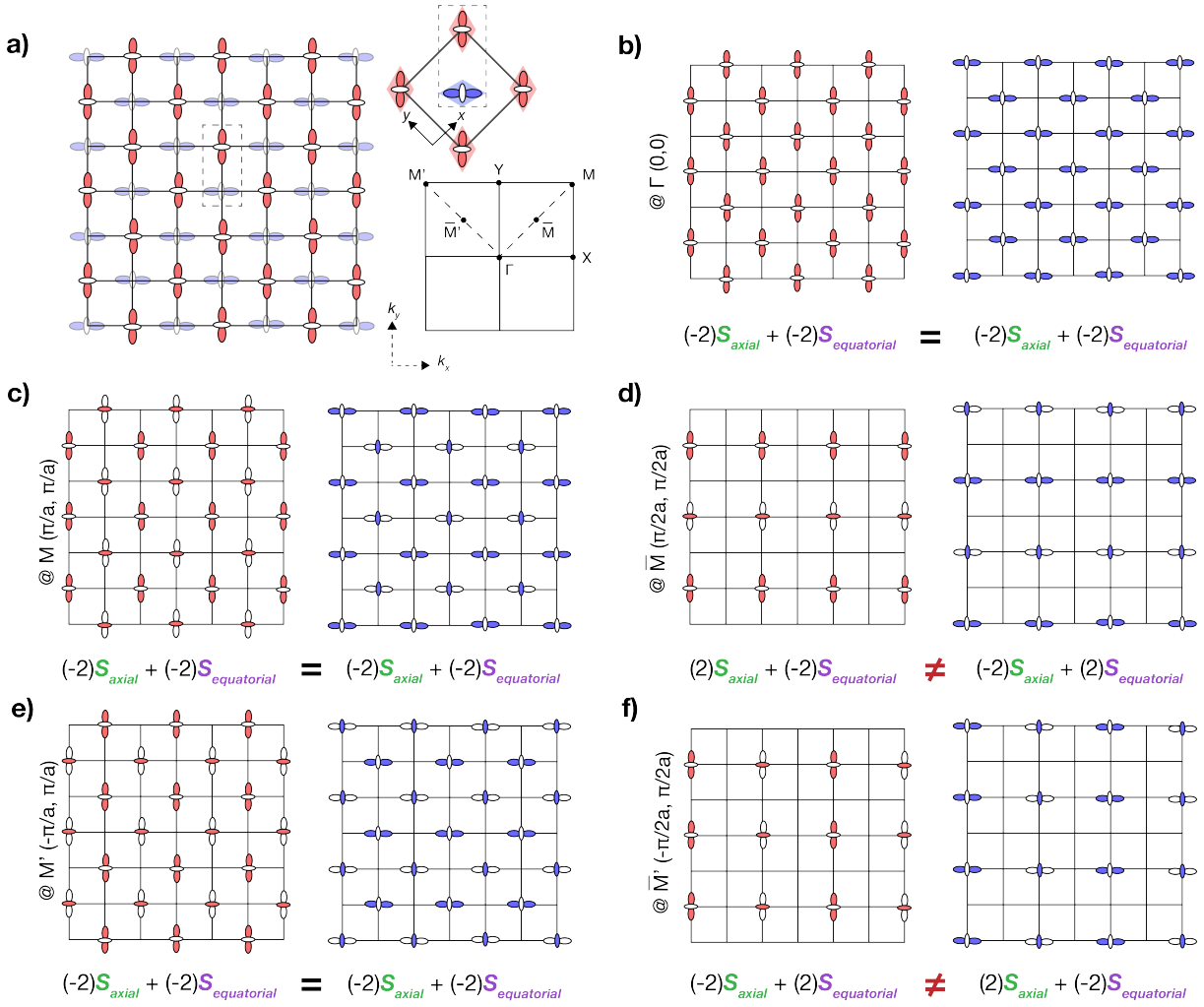

Figure 5: Description of the orbital phases at different high symmetry points in the Brillouin zone for our rutile toy model. a) Shows the spin–up and spin–down sublattices, colored as red and blue respectively, with metal centers decorated by d_{z^2} orbitals. The xy coordinates of the basis, highlighted in a grey dotted box, and high symmetry points of a square sublattice BZ for each independent square sublattice are also shown. b-f) Metal–metal interactions, based on d_{z^2} orbitals, are distinguished by axial- or equatorial-type interactions. Equivalent or inequivalent interactions between the spin–up (red) and spin–down (blue) layers are qualitatiely evaluated for Γ (0, 0), M $(\frac{\pi}{a}, \frac{\pi}{a})$, $\bar{\text{M}}$ $(\frac{\pi}{2a}, \frac{\pi}{2a})$, M' $(\frac{-\pi}{a}, \frac{\pi}{a})$, and $\bar{\text{M}}$' $(\frac{-\pi}{2a}, \frac{\pi}{2a})$, respectively.

independent square sublattices of antiparallel spins. The high-symmetry coordinates (k_x, k_y) of our BZ in reciprocal space are thus Γ (0, 0), $\bar{\text{M}}$ ($\frac{\pi}{2a}$, $\frac{\pi}{2a}$), M ($\frac{\pi}{a}$, $\frac{\pi}{a}$); at these high symmetry points we will apply phase factors determined by $e^{i\mathbf{kr}}$, according to Bloch's theorem. At Γ (Figure 5b), the phase factor is determined by the reciprocal space coordinates (0,0), and orbitals propagate in the x and y direction without phase inversion. Accordingly, at Γ in-phase ("bonding") interactions populate the nearest-neighbor axial and equatorial directions of the d_{z^2} orbitals for both spin-up and spin-down sublattices, resulting in spin degeneracy. At M, the phase factor is determined by ($\frac{\pi}{a}$,$\frac{\pi}{a}$). In this case, the phase inversion introduces out-of-phase ("antibonding") interactions uniformly along all four diagonal directions. In-phase interactions are preserved for both axial and equatorial directions in the spin-up and spin-down lattices, which once again leads to spin degeneracy. At the intermediate point $\bar{\text{M}}$, the phase factor is determined by ($\frac{\pi}{2a}$, $\frac{\pi}{2a}$), introducing nodes into the treatment of the wave function before applying phase inversion. For the spin-up sublattice, the orbitals display out-of-phase interactions along the axial direction and in-phase interactions along the equatorial direction. The converse is true for the spin-down sublattice. This discrepancy, introduced by in-phase and out-of-phase interactions disparately affecting orbitals on each sublattice, creates a break in band degeneracy at $\bar{\text{M}}$, leading to a local region of spin-split bands.

The bands splitting along Γ-M represent only half of the fourfold bands derived from a two-orbital basis. Unlike other momentum-split band phenomena, a unique aspect of spin-split bands in altermagnets (that have apparent momentum-space dependence yet are not formally momentum-split) is that this splitting is not due to second-order perturbative effects, such as the SOC-induced Rashba-Dresselhaus splitting.[39–43] In an analogous derivation of momentum splitting due to the Rashba-Dresselhaus effects, SOC is introduced after determining the bands' dispersion and position from the noncentrosymmetric crystal lattice. That is, SOC is "turned on" to observe momentum splitting.[39,40] In altermagnets, however, momentum splitting arises directly from global lattice symmetries, therefore, the path along Γ-M only accounts for half of the bands, and the fourfold degeneracy is recovered across the

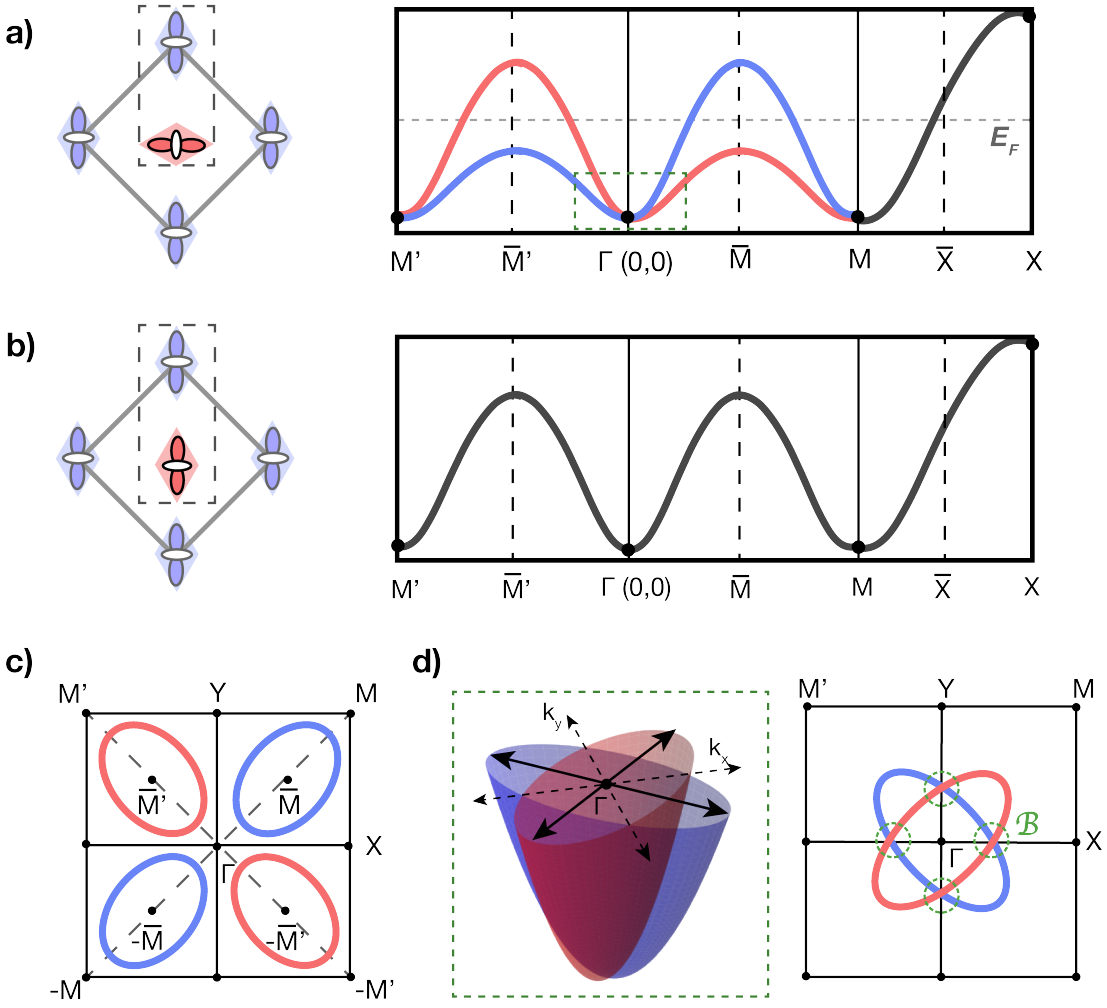

Figure 6: Electronic band dispersion of an altermagnet and conventional antiferromagnet. a) Depiction of an altermagnetic unit cell decorated with d_{z^2} orbitals, along with its qualitative electronic band dispersion, where the Fermi level (E_{F}) is indicated. b) Conventional antiferromagnet unit cell decorated with d_{z^2} orbitals and its corresponding electronic band dispersion that shows both the spin–up and spin–down bands as degenerate. c) Qualitative two-dimensional Fermi surface of a) that depicts a d-wave symmetry at (E_{F}). d) Left:Quadratic, d-wave band dispersion around Γ, shown in the green dashed box in a), emphasizes the symmetry of the nodal planes. Right: Avoided crossings, which in the presence of SOC would lead to Berry curvature ($\mathcal{B}$) hotspots, are marked by green dashed circles along the Γ-X and Γ-Y directions.

full first Brillouin zone.

To recover a fourfold degeneracy of bands from a basis of two d_{z^2} orbitals, we analyze the dispersion along Γ-M' in Figures 5e and 5f. A similar treatment to that described above for Γ-M is applied here, but the orbital phases are shifted along the x direction to reflect the negative component of the phase factor introduced by M' = $(-\frac{\pi}{a}, \frac{\pi}{a})$ and $\bar{\text{M}}$' = $(-\frac{\pi}{2a}, \frac{\pi}{2a})$. The resulting energy difference from broken band degeneracy at $\bar{\text{M}}$' is equivalent to that of $\bar{\text{M}}$, but the sign for the respective energy of the spin-up and spin-down bands switches due to the inversion of bonding and antibonding interactions.

Finally, we present the resulting simplified electronic band diagram derived from the altermagnetic toy model in Figure 6a. High symmetry points of the Brillouin zone at Γ and M are spin band degenerate, and the intermediate points along Γ-M and Γ-M' reveal momentum split bands. In an analogous antiferromagnetic toy model (Figure 6b), the compensated spins would retain degeneracy because of real-space sublattices that transform by translation. By taking an arbitrary cut to represent the Fermi level in the band diagram of Figure 6a, we observe the d-wave magnetic symmetry of the Fermi surface predicted for altermagnetic rutiles in Figure 6c. Additionally, the symmetry imposed by altermagnetic band splitting generates nodally degenerate planes, which, in the case of the toy model, occur along Γ-X and Γ-Y in the nonrelativistic band structure. Quadratic, d-wave band dispersion around the gamma point, marked by the green dashed box in Figure 6a and depicted as 3-dimensional band valleys in Figure 6d, highlight the symmetry of these nodal planes. In real material systems with SOC, the nodal planes along k_x and k_y become regions of avoided crossings for spin-up and spin-down bands, thus giving rise to symmetry-defined Berry curvature ($\mathcal{B}$) hotspots, as we discuss below.[12]

The toy model used to derive altermagnetic spin-splitting is predicated on the ideal scenario where SOC is omitted. As we have already alluded to, SOC is not negligible in real material systems. Thus, altermagnetism is reasonably expected to be more complicated than this simple, nonrelativistic picture. In one view, the nonrelativistic limit used to de-

rive the altermagnetic band structure generates a parent phase from which the features of altermagnetism may emerge. In instances where the spin-orbit interaction induces canting, the altermagnetic parent phase is not necessarily extinguished despite its coexistence with a weak ferromagnetic component. Ultimately, if the canting retains the same mapping of spin symmetries localized in rotated environments, similar spin splitting is expected to occur.[44–46]

The Anomalous Hall Effect

One measurable probe of broken time-reversal symmetry is the observation of an anomalous Hall effect (AHE). This phenomenon serves as a connection between electronic transport and intrinsic electronic band structure properties such as NRSS and topology. The AHE can, therefore, provide a powerful way to identify NRSS in materials, including altermagnets. We now discuss the origin of this effect in terms of the real space spin-structure of a magnetic material. In the next section, we discuss its microscopic origin in the electronic band structure and a property known as the Berry phase.

When an electric current flows through a conductor in the presence of a perpendicular magnetic field, the longitudinal current is deflected by the magnetic field, resulting in a transverse resistivity that depends on the charge carrier density of the conductor and the magnetic field strength. This is the Hall effect (or "ordinary" Hall effect). Ferromagnets display an additional, larger effect that appears proportional to the magnetization and therefore may arise in the absence of an external magnetic field in the presence of nonzero magnetization. This "anomalous" Hall effect was thus originally thought to be an exclusive hallmark of ferromagnets/ferrimagnets arising from uncompensated spins.[47] More recently, it has been shown that the AHE can be present in materials with no internal magnetization, including altermagnets, as long as specific symmetries are broken.[12,13,30,48]

Just as symmetries define an altermagnet (as explained previously), symmetries of the magnetic structure also determine whether or not there is an AHE. This makes the AHE one way to experimentally measure the presence, and consequences, of altermagnetic sym-

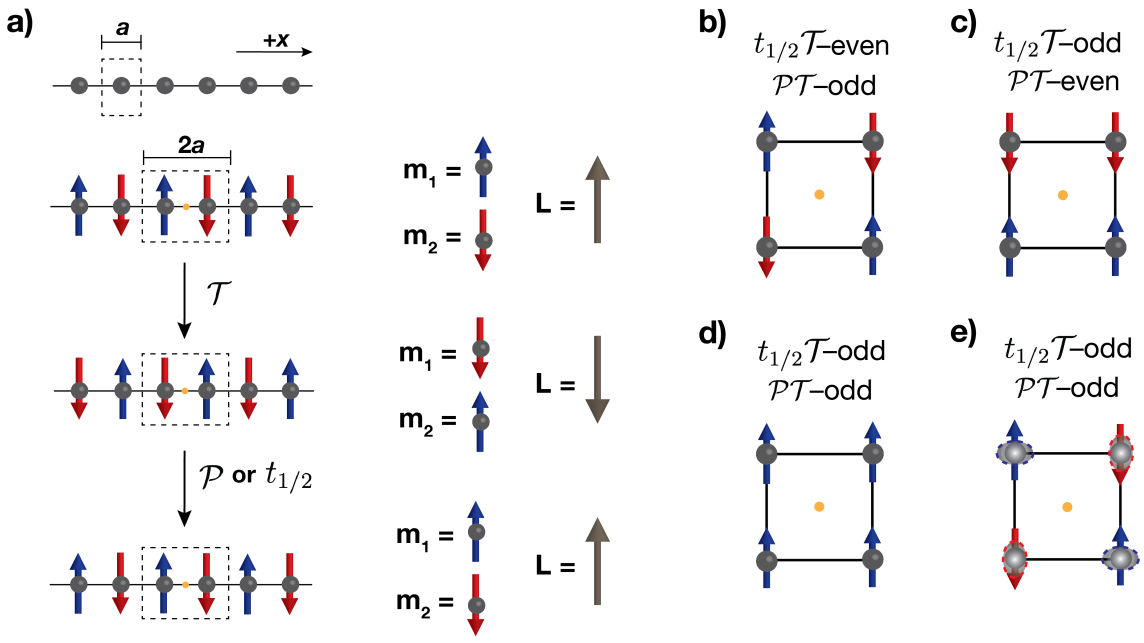

Figure 7: a) Summary of how the Néel vector changes orientation depending on the symmetry operation, in this case, time-reversal, translation, and inversion, on a 1D antiferromagnetic chain. b-e) Summary of the different spin orientations and their magnetization density that break or preserve $t_{1/2}\mathcal{T}$ and $\mathcal{PT}$.

metry. To understand the symmetries that allow an AHE, we note that irrespective of origin, we can describe the AHE by an order parameter termed the Hall vector, $\mathbf{h}$, such that $\mathbf{j}_{\text{Hall}} = \mathbf{h} \times \mathbf{E}$, where $\mathbf{j}_{\text{Hall}}$ and $\mathbf{E}$ are the Hall current and the electric field, respectively.[20,30] Importantly, $\mathbf{h}$ breaks time reversal symmetry ($\mathbf{h}$ is $\mathcal{T}$-odd), and so for any material to display a non-zero $\mathbf{h}$, that material must also break $\mathcal{T}$ symmetry.[30,49] As we show below, although spin compensated materials break $\mathcal{T}$ microscopically/locally, we need to consider translation and inversion symmetry in conjunction with $\mathcal{T}$ to understand whether such a system would exclude $\mathbf{h}$ and accordingly, the AHE. To start, we note that the order parameter that characterizes collinear antiferromagnets and altermagnets is the Néel vector, $\mathbf{L}$:[30]

$$\mathbf{L} = \sum_i \mathbf{m}_i - \sum_j \mathbf{m}_j$$

where $\mathbf{m}_i$ and $\mathbf{m}_j$ are spins from different magnetic sublattices in the magnetic unit cell.[30,50]

We now consider a simple 1D antiferromagnetic chain (Figure 7a). The $\mathcal{T}$ operation flips the sign of $\mathbf{L}$ since $\mathbf{m}_{i,j}$ is a $\mathcal{T}$-odd vector. However, the lattice transposing $t_{1/2}$ operation

(where $t_{1/2}$ is a half-unit cell translation of the antiferromagnetic structure when considering a two-sublattice collinear antiferromagnet—the magnetic unit cell is double the unit cell of the crystal lattice) then flips the signs of $\mathbf{m}_{i,j}$ (and thus the sign of $\mathbf{L}$) back, as shown in Figure 7a. Thus, $\mathbf{L}$ remains invariant under $t_{1/2}\mathcal{T}$. Since $\mathbf{h}$ changes sign due to $t_{1/2}\mathcal{T}$—$\mathbf{h}$ is invariant under $t_{1/2}$ operations since translation does not change momentum space features[30,48]—a $t_{1/2}\mathcal{T}$-symmetric antiferromagnetic material will exclude $\mathbf{h}$ and display no AHE. Likewise, we can consider the effect of the inversion operation ($\mathcal{P}$), in combination with time reversal, (*i.e.* $\mathcal{PT}$). We note that as a rank-2 tensor, the Hall conductivity tensor is centrosymmetric even if the material is non-centrosymmetric (as in the case of $V_{1/3}NbS_2$).[51,52] Applying the inversion operator on an individual spin changes its coordinates but not the direction of the spin: $\psi(x, y, z, \uparrow) \rightarrow \psi(-x, -y, -z, \uparrow)$, resulting in a change in sign of $\mathbf{L}$ as shown in Figure 7a. This simple analysis in 1D shows that for a spin compensated material, if the Néel vector is $t_{1/2}\mathcal{T}$- or $\mathcal{PT}$-invariant, the AHE cannot be observed.[30]

In two dimensions (Figure 7b-e) we can also show that conventional collinear antiferromagnets (Figure 7b,c) might preserve either $t_{1/2}\mathcal{T}$ or $\mathcal{PT}$ and therefore should not host the AHE. However, when the symmetry of the crystal is such that the electron density of spin up and spin down sites are related by rotation (Figure 7e), both $t_{1/2}\mathcal{T}$ and $\mathcal{PT}$ are broken. It is this feature of altermagnets that can give rise to a non-zero $\mathbf{h}$. An analogous symmetry analysis shows how the AHE can also be observed in ferromagnets (Figure 7d). It can also be shown that the AHE may likewise be observed in some non-collinear antiferromagnets,[30,47,48] but that lies out of the scope of this Perspective. While altermagnets have the potential to manifest an AHE based on these symmetry considerations, it is important to note that the observation of the AHE in altermagnets also depends on the direction of Néel vector with respect to the symmetry of the crystal structure.[53,54]

The AHE and geometric Berry phase

At a microscopic level, the presence of an AHE can be related to the concept of the geometric Berry phase[55,56]—a concept that is manifest even in classical mechanics as the change in a pendulum's plane of motion due to the earth's rotation (i.e., the Hannay angle in the Foucault pendulum)[57,58] and is relevant to many other quantum mechanical systems.[59–62] In the context of electronic transport in crystals, as an electron in the bands of a material moves through a closed loop of momentum space (due to the application of an external magnetic or external electric field), the electron will pick up a Berry phase that is defined by the band structure. Specifically, the property of the electronic band structure that governs the Berry phase is called the Berry curvature, which depends on the symmetry and topology of the electronic band structure. This Berry curvature is proportional to the intrinsic AHE, thus establishing a direct connection between variables that are measurable in electrical transport and the spin-split band structure of altermagnets.

Mathematically, the association of the Berry phase with the microscopic origin of the AHE can be understood by recognizing that the antisymmetric Hall conductivity, σ_{xy}^{a}, has an intrinsic origin:

$$\sigma_{xy}^{a} = -\frac{e^2}{\hbar}\Sigma_n \int_{\mathrm{BZ}} \frac{d^3k}{(2\pi)^3} f[\varepsilon_n(\mathbf{k})]\ \mathcal{B}_n^z(\mathbf{k})$$

Here $f[\varepsilon_n(\mathbf{k})]$ is the Fermi–Dirac distribution function, $\varepsilon_n(\mathbf{k})$ is the energy of the Bloch state in band n with crystal momentum $\mathbf{k}$, and $\mathcal{B}_n^z(\mathbf{k})$ is the aforementioned Berry curvature. The Berry curvature is related to the Berry phase by the Berry connection (or Berry potential), $\boldsymbol{A}_n(\mathbf{k})$ as

$$\mathcal{B}_n^z(\mathbf{k}) = \nabla_{\mathbf{k}} \times \boldsymbol{A}_n(\mathbf{k})$$

where the integral of the Berry connection through a closed loop is the Berry phase, γ:

$$\gamma = \oint\ \boldsymbol{A}_n(\mathbf{k})\ d\mathbf{k}$$

In materials that break time-reversal symmetry, the AHE is allowed by symmetry, and a finite Hall conductivity may be explained by a finite integral of the Berry curvature. In materials that do not break time reversal symmetry, $\mathcal{B}_n(\mathbf{k}) = -\mathcal{B}_n(-\mathbf{k})$ and so the integral of $\mathcal{B}_n(\mathbf{k})$ over the BZ leads to a vanishing σ^a_{xy}. In some band structures, the presence of SOC can lead to Berry curvature hotspots around avoided crossings (where spin-up and spin-down bands intersect) that can lead to a robust Hall conductivity. Indeed, even in the absence of ferromagnetic order, avoided crossings such as those found at Weyl nodes will produce a Hall conductivity.[47,63–65]

In the case of conventional antiferromagnetism, as explained above, although time-reversal symmetry is broken microscopically, the underlying symmetries (such as translation and inversion symmetry) that relate the spin sublattices exclude the AHE.[48] In contrast, since these symmetries remain broken in altermagnets, a finite Hall conductivity can be preserved by a non-zero integral of the Berry curvature, though this will also depend on the orientation of the Néel vector itself.[12,30,31,44,66] In addition, the symmetry-imposed alternation in spin polarization produces avoided crossings at certain high symmetry points of the BZ (Γ, M, and M' in the case of the toy model shown in Figure 6b) and at nodal planes (Figure 6d) that due to spin–orbit coupling lead to local exacerbation in the Berry curvature.[12,30] Altermagnets are therefore a platform for realizing and exploring Berry phase phenomena, including quantum Hall behavior and resultant nondissipative transport, at high temperatures.[30]

Altermagnets for spintronics

The electrical manipulation of ferromagnetic order is the basis for commercialized magnetic random access memory (MRAM).[67–70] Early MRAM schemes used Oersted fields generated in current carrying lines to flip the magnetic moments of a soft ferromagnetic layer in crossbar arrays of magnetic bits comprised of magnetic tunnel junctions (MTJs).[71] Limitations on

bit density (due to incidental switching of closely spaced MTJs by the Oersted fields in the bit lines) and energy efficiency were overcome by the development of MRAM devices that use the spin transfer torque (STT) mechanism (STT-MRAM).[72–75]

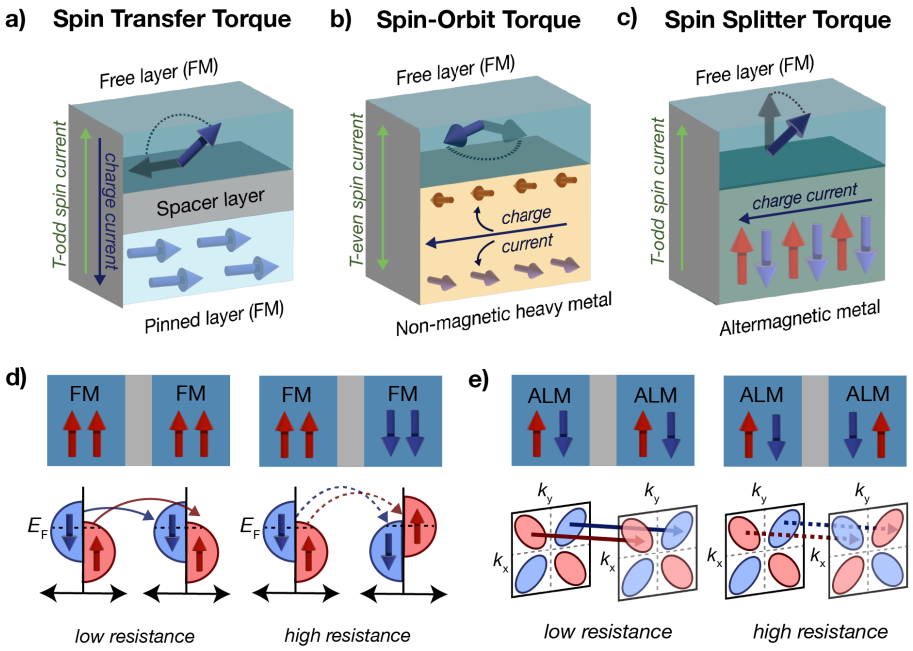

Figure 8: a) Spin transfer torque device geometry where a hard ferromagnetic layer (the pinned layer) is layered on another "free" ferromagnet with a spacer layer in-between. The polarization of the free layer is manipulated by the direction of spin-polarized current from/through the pinned layer. b) Spin-orbit torque device geometry where current flow through a heavy non-magnetic metal, such as Ta, is used to switch the polarization of an adjacent free ferromagnetic layer. c) Spin splitter torque device geometry where the spin polarization generated from current flow through an altermagnet is used to flip the direction of the adjacent free ferromagnetic layer. d) A typical density of states diagram for a ferromagnetic tunnel junction (FM-TJ), depicting the difference in tunneling magnetoresistance for two schemes where the spins of the ferromagnets are parallel (left; low resistance) or anti–parallel (right; high resistance). e) AFM/ALM-TJ device geometries showing the momentum-space alignment of spin-split bands in a non-collinear AFM or ALM. When the Néel vectors of the magnetic layers are parallel (left) the phases of the Fermi surfaces from the altermagnets match, leading to a low resistance state. When the Néel vectors are anti–parallel (right) the phases of the Fermi surfaces do not match, leading to a high-resistance state.

In STT-MRAM, switching of the soft ferromagnetic layer (the "free" layer) of the MTJ is accomplished by a spin-polarized current that is generated as charge flows through a hard ferromagnetic metal, called the pinned/fixed layer.[72,73] Beginning in an antiparallel alignment

of moments in pinned and free layers, after tunneling across the insulating spacer, the spin-polarized current transfers spin angular momentum to the free layer, exerting a torque on the moments in the free layer that results in an reversal of the magnetic moments in this free layer to bring them into alignment with those of the fixed layer (Figure 8a). This produces a low resistance state of the MTJ. To flip magnetization of the free layer, a current flows in the opposite direction. Now, the fixed layer serves to preferentially filter through electrons bearing spins aligned parallel to its own polarization. This process leads to an accumulation of the opposite spin angular momentum in the free layer, which eventually flips the moments back so that the free and fixed layers are returned to an anti-parallel configuration and enables a high resistance state. Although the STT approach is more energy-efficient and faster than the Oersted field mechanism, STT uses the same current path for both reading and writing (with current flowing perpendicular to the layer interfaces). This can cause incidental switching during readout and therefore compromises information stability.[75]

An alternative scheme is based on the spin–orbit torque (SOT) switching mechanism.[76–79] Here, current flow occurs through a nonmagnetic heavy metal (e.g. Pt, Ta) layer parallel to the free layer. The spin Hall effect[80] in the nonmagnetic layer produces a spin current such that the spin current, the electric field that produces the charge current, and the spin direction are mutually orthogonal. The spin Hall effect thus serves to inject spins upwards into the free layer as charge current flows longitudinally through a nonmagnetic line below. Combined with the Rashba-Edelstein effect[81,82] at the interface, current flow through this nonmagnetic layer exerts a torque on the moments in the free layer that allows the moments in the MTJ to be manipulated into parallel or antiparallel orientations (Figure 8b). One benefit of SOT as the switching mechanism is the decoupling of write-in and read-out current paths. However short spin diffusion lengths, limited charge-to-spin conversion efficiencies, and high resistivities of the spin source materials present challenges to device performance.[75,83]

Altermagnets now provide a new mechanism for the generation of spin currents that do not rely on spin-orbit coupling, and may overcome some of these limitations of SOT.

In altermagnets, current flow perpendicular to the Néel vector is proposed to generate a strong spin current along the Néel vector direction, a mechanism termed spin splitter torque (SST)[12,83,84] as depicted in Figure 8c. This SST process combines some of the advantages of STT and SOT (namely, being non-relativistic in origin and allowing a decoupling of read and write paths) and may allow ALMs to serve as highly efficient spin source materials for all-electrical MRAM technologies. However, generation of the spin current in the desired direction requires specific alignment of the crystal axes of the altermagnet with the MTJ interfaces.

Among the magnetic memory elements discussed so far, only those based on ferromagnetic MTJs have been commercially implemented to date. In FM-MTJs, parallel and antiparallel alignments of fixed and free FM layers lead to respective low- and high-resistance states for electron tunneling between the FMs. This can be understood simply as a result of changing the spin-dependent density of electronic states, DOS (Figure 8d). The intrinsic limits on magnetization dynamics in ferromagnets (and therefore limits on switching speeds) have led to intense contemporary interest in antiferromagnetic spintronics, which in principle, could display much faster switching dynamics.[85,86] To understand how magnetically compensated systems such as non-collinear AFMs or ALMs can be used in MTJs despite spin-degenerate DOS, it is helpful to view electron tunneling across an MTJ in momentum space. As we have already discussed, NRSS in ALMs leads to anisotropic Fermi surfaces. Using a *d*-wave altermagnet as an example in Figure 8e, alignment of the spin sub-bands in momentum space across the MTJ leads to a low resistance state. However, when the Néel vector of one altermagnetic layer is rotated 180° the spin sub-bands are misaligned in momentum space, leading to a high resistance state.[85] Specific mechanisms for switching the altermagnet Néel vector may depend on the crystal structure, magnetocrystalline anisotropy, and other electronic properties of the material, but precedent exists for electrical manipulation of Néel vectors and other order parameters in antiferromagnets; examples include CuMnAs, Mn_2Au, and $Fe_{1/3\pm\delta}NbS_2$.[8,87,88]

In addition to MTJ-based memories, there are proposals to combine altermagnets with superconductors as a new memory platform.[89] In the proposed architecture, an altermagnet is adjacent to a superconductor, or a superconductor is sandwiched between two altermagnets, where the phases of the altermagnet Fermi surface modulates the critical temperature, T_c, of the superconductor. The proximity of these systems is allowed due to the absence of stray fields in altermagents.

Together with non-collinear AFMs, NRSS in altermagnets offers distinctive possibilities for novel spintronic device schemes that could lead to fast switching memories and ultralow power micro-electronic systems. However, further work is still required to more deeply understand the electronic properties of altermagnets and the exciting possibilities for magnetic devices. Expanding the library of ALMs will be a key step forward. Next, we provide a short survey of some proposed ALMs across a few materials classes with disparate structures/symmetries, and highlight some key experimental studies on these systems so far.

Synopsis of candidate altermagnetic materials

Altermagnetism has been proposed in a variety of structural hosts, including both two-dimensional (2D) and three-dimensional (3D) systems, in noncentrosymmetric and centrosymmetric crystal lattices, and across various Bravais lattice types. The concept also extends to electronic insulators, semiconductors, metals, and superconductors.[12] Here, we describe the symmetries of several candidate altermagnets and summarize key experimental findings that provide evidence for or against their altermagnetic ground state.

Rutile RuO_2

Ruthenium dioxide (RuO_2) crystallizes in a tetragonal unit cell with space group $P4_2/mnm$, shown in Figure 9a. Highlighted in Figure 9b, the distorted RuO_6 octahedra surrounding Ru_A and Ru_B centers transform by a $C_{4z}\mathbf{t}$ real-space rotation. This operation corresponds to

a C_4 rotation around the crystallographic c-axis followed by a half-unit cell translation along the [111] direction. The spin configuration, also depicted in Figure 9b, assumes a simple A-type pairing where opposite magnetic moment vectors are related by a C_2 rotation. Under this formalism, the combined $[C_2||C_{4z}\mathbf{t}]$ non-relativistic space group results in purported d-wave altermagnetic symmetry in RuO_2.

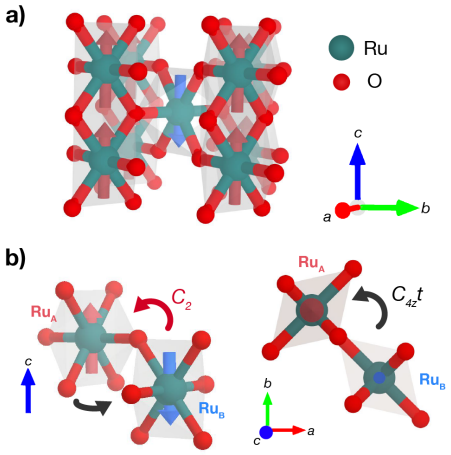

Figure 9: a) The crystal structure of RuO_2 with the $P4_2/mnm$ space group and the spins at each Ru site. b) Depicts the $[C_2||C_{4z}\mathbf{t}]$ symmetry of the opposite spin sublattices (Ru_A and Ru_B).

Several works have used RuO_2 to illustrate the fundamental symmetries that result in altermagnetism,[12,13] which relies on the validity of the spin and crystal configurations described above. However, the magnetic ground state of RuO_2 remains a topic of significant debate. Intuitively, the $4d^4$ electron configuration of Ru^{4+} results in a fully paired spin configuration, which implies a diamagnetic ground state under the reduced symmetry of a distorted octahedral environment.[38] An antiferromagnetic ground state was initially proposed through DFT + U calculations and supported by magnetic susceptibility and neutron scattering measurements.[90] Following the adoption of RuO_2 as the "prototypical altermagnet", the observation of an anomalous Hall effect catapulted RuO_2 into the central limelight of this field.[91] Ongoing efforts aim to resolve the question of the magnetic ground state in RuO_2. So far, muon spin rotation experiments indicate that the reported altermagnetic order is unlikely to exist in the bulk crystal,[92] and other experimental reports including neu-

tron diffraction[93] and spin-angle resolved photoemission spectroscopy[94] also challenge the proposed altermagnetic order.

Hexagonal semiconductor MnTe

Manganese telluride (α-MnTe) crystallizes in the hexagonal NiAs structure type (space group $P6_3/mmc$). It is a magnetic semiconductor with a moderate indirect band gap of 1.27 to 1.46 eV.[95] Comprehensive analyses, including neutron diffraction, magnetometry, magneto-transport, and DFT+U calculations, reveal that MnTe exhibits an A-type magnetic ground state below a Néel temperature (T_N) of 310 K.[96–99] Below this critical temperature, spins align ferromagnetically along the $[1\bar{1}10]$ direction and antiferromagnetically between adjacent c-axis layers. The structural and magnetic unit cell of α-MnTe is shown below in Figure 10a. Due to inequivalent stacking of octahedral environments, the opposite spin sublattices at Mn_A and Mn_B (Figure 10b) are related by a sixfold rotation or mirror operation. This corresponds to the nonrelativistic space group operation $[C_2||C_{6z}\mathbf{t}]$, describing the twofold rotation of A-type spins and a sixfold rotation of the real-space environment followed by translation along the crystallographic c axis. These symmetries result in antisymmetric spin bands and a g-wave altermagnetic phase.

MnTe is a key material in the experimental investigation of altermagnetism using spin angle-resolved photoemission spectroscopy (SARPES), which provides direct evidence of spin-split spin bands. The method relies on angle-resolved photoemission spectroscopy (ARPES) to reconstruct a material's electronic structure using the kinetic energies and collection positions of photo-emitted electrons, which correspond to binding energies at specific momentum values in reciprocal space. This technique enables selective mapping of a k_x-k_y surface at a fixed k_z in the Brillouin zone (BZ).[100] In complementary SARPES, a polarized detector can differentiate spin-up from spin-down bands.[34,101] Direct, experimental evidence of spin-split bands through spectroscopic imaging is in some ways more definitive evidence of altermagnetism than the indirect evidence from the observation of an anomalous Hall

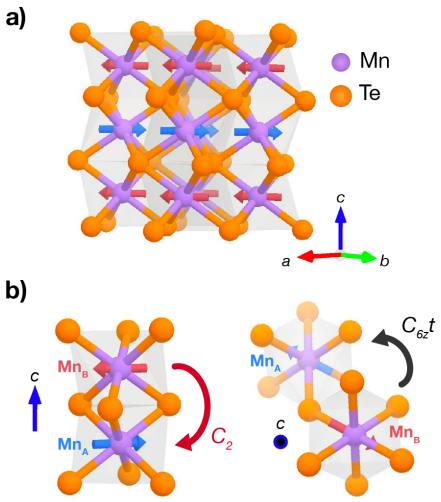

Figure 10: a) The crystal structure of MnTe with the $P6_3/mmc$ space group and the spins at each Mn site. b) Depicts the $[C_2||C_{6z}\mathbf{t}]$ symmetry of the opposite spin sublattices (Mn_A and Mn_B)

current. However, experimental verification via SARPES is challenging due to the rarity of materials with significant spin splitting and the potential for multiple magnetic domains to nullify a measurable spin polarization.[102]

Several properties make α-MnTe suitable for observing altermagnetism through ARPES and SARPES. For one, the calculated valence band spin splitting of 1.1 eV is among the largest in known altermagnetic materials.[12] A large spin splitting implies that MnTe's spin bands can be distinguished with ARPES alone, even without spin resolution.[13] Additionally, MnTe is a candidate for single-domain altermagnetism, which is supported by predictions of domain wall formation perpendicular to the ab plane[102] and the demonstrated ability to reorient domains by cooling under an applied field.[103,104] However, detecting a spin-split signal requires instruments with spot sizes smaller than the average domain size ($\sim$30 nm in thin film MnTe and $\sim$10 μm in bulk MnTe) or the fortunate occurrence of a dominant easy-axis Néel vector in a multi-domain probe.[44] Furthermore, ARPES measurements are surface-sensitive, and a (0001) terminated MnTe surface shows local ferromagnetism, adding further complexity to data analysis and interpretation.[34]

In MnTe, the spin-split bands reside outside the spin-degenerate nodal planes in the non-

relativistic limit (without SOC), corresponding to a cut parallel to the Γ-M direction.[44,105] Measured soft X-ray ARPES data outside of MnTe's nodal planes has shown a strong signature of altermagnetic splitting below the magnetic ordering temperature, reaching the half-eV scale in thin-film MnTe. The signal disappears along the nodal spin-degenerate planes.[44] The confirmation of this signature in bulk samples, using UV-SARPES, has revealed that the opposite spin polarizations have asymmetric momentum dependence. These measurements are among the first instances of direct experimental evidence for strong, nonrelativistic altermagnetic lifting of Kramer's spin degeneracy.[44]

Measurements of the electronic band structure within the nodal plane, both along k_x (Γ-K) and k_y path (Γ-M), revealed quadratic band dispersion and a weakly lifted Kramer's degeneracy around the Γ point. This spin-splitting is small at Γ and sees a nonlinear rise towards K and M points. Confirmed in both experiment and theory, it has been suggested that this weak, relativistic lifted Kramers spin degeneracy (LKSD) arises due to a SOC-induced net magnetization in MnTe, thus enabling a canting of the sublattice moments towards the c-axis. In this case, the interplay between altermagnetism and SOC generates a spin polarization of bands orthogonal to the direction of the magnetic-order vector, and as a result, spin-splitting can be observed along regions that are predicted to be spin-degenerate through nonrelativistic symmetry analysis. These weakly spin-split bands lack constant and linear terms commonly used to describe spin-splitting in conventional ferromagnets, or in systems with broken inversion symmetry, thus highlighting the key distinction of an altermagnetic mechanism of LKSD.[44,106]

The manifestation of both strong (without SOC) and weak (with SOC) altermagnetic LKSD may offer distinct applications. Strong altermagnetic LKSD is proposed to be valuable for quantum devices in novel architectures. Weak altermagnetic LKSD, as observed in thin-film MnTe, supports dissipationless Anomalous Hall transport, driven by Berry-phase physics.[107–109]

Intercalated Transition Metal Dichalcogenides (TMDs): $V_{1/3}NbS_2$ and $Fe_{1/4}NbS_2$

Magnetic intercalated TMDs encompass materials of the form T_xMCh_2 (T = intercalant M = transition metal Ch = chalcogenide, where spin bearing ions, T, occupy the octahedral sites of a parent TMD compound, such as NbS_2, and thus introduce magnetic order. Crystallographic superlattices form at intercalant stoichiometries of $x = 1/4$ and $1/3$, resulting in $2a \times 2a$ and $\sqrt{3}a \times \sqrt{3}a$ superlattices respectively, where a is the lattice constant of the parent TMD.[51] Here, we highlight two altermagnetic candidates that emerge from this class of materials.

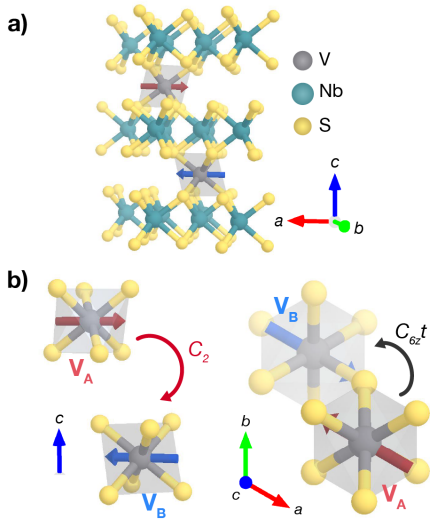

Figure 11: a) The crystal structure of $V_{1/3}NbS_2$ with the $P6_322$ space group and the spins at each V site. b) Depicts the $[C_2||C_{6z}\mathbf{t}]$ symmetry of the opposite spin sublattices (V_A and V_B)

$V_{1/3}NbS_2$ forms a $\sqrt{3}a \times \sqrt{3}a$ superlattice, characterized by a hexagonal unit cell and a noncentrosymmetric space group of $P6_322$, illustrated in Figure 11. The octahedral ligand coordination surrounding V_A and V_B spin centers, depicted in Figure 11b, are related by a $C_{6z}\mathbf{t}$ operation, which corresponds to a C_6 rotation combined with a translation parallel to the [111] direction. Although experimental confirmation of the magnetic unit cell remains inconclusive,[110,111] the quenched orbital angular momentum of V^{3+} ions suggests that the

material should adopt an A-type collinear spin pairing with spin symmetry C_2 (Figure 11b). In this case, the presumed $[C_2||C_{6z}\mathbf{t}]$ nonrelativistic spin group symmetry leads to g-wave spin splitting in the electronic band structure.[12]

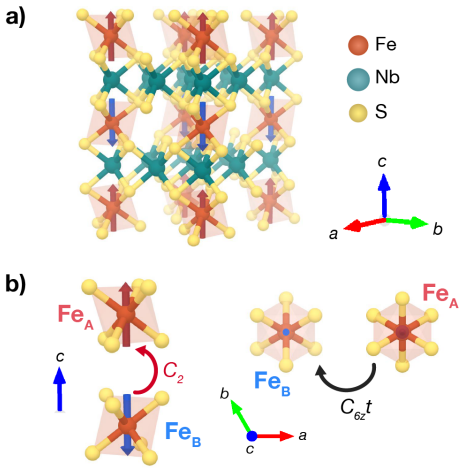

Figure 12: a) The crystal structure of $Fe_{1/4}NbS_2$ with the $P6_3/mmc$ space group and spins located at each Fe site. b) Depicts the $[C_2||C_{6z}\mathbf{t}]$ symmetry of the opposite spin sublattices (Fe_A and Fe_B).

$Fe_{1/4}NbS_2$ forms a $2a \times 2a$ superlattice where the hexagonal space group of the parent TMD, $P6_3/mmc$, is retained (Figure 12).[112] The material also retains centrosymmetry. Fe_A and Fe_B spin centers, depicted in Figure 12b, share the $[C_2||C_{6z}\mathbf{t}]$ nonrelativistic spin group symmetry of the $\sqrt{3}a \times \sqrt{3}a$ superlattice.

The broader class of intercalated TMDs includes several MCh_2 compounds of the $2H$ polytype where the spin-bearing atoms occupy octahedral sites, including first-row transition metals V, Cr, Mn, Fe, Co, and Ni. As demonstrated above, the $2a \times 2a$ and $\sqrt{3}a \times \sqrt{3}a$ superlattices of intercalated TMDs support the symmetry considerations for altermagnetism. In the event of A-type AFM interactions, which meets the C_2 rotation criteria in spin space, these materials are candidates for altermagnetism. Recent experiments do show evidence for altermagnetism in the Co-intercalated compounds.[54,113]

Insulating Perovskite $LaMnO_3$

Ruddlesden-Popper phases and their perovskite end members are often suitable candidates for hosting altermagnetism.[11,114] Many candidates have thus far been identified through first-principles and symmetry-group analyses. Here, we will examine and contextualize these relevant symmetries in $LaMnO_3$.

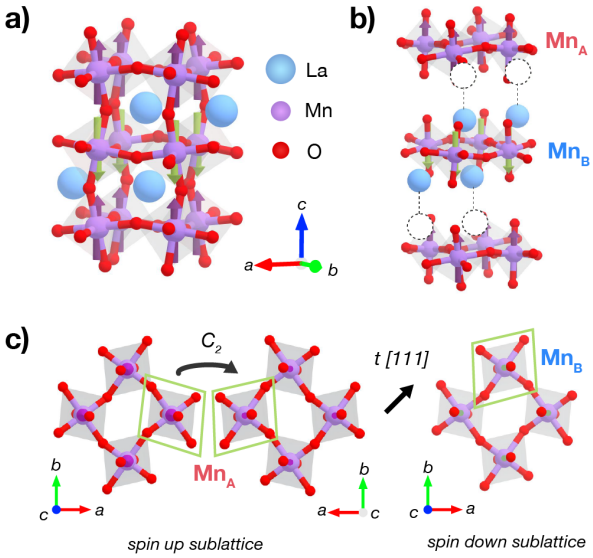

Figure 13: a) The crystal structure of $LaMnO_3$ with the *Pbnm* space group and the spins at each Mn site. b) To illustrate the $[C_2||C_{2y}\mathbf{t}]$ symmetry the layers are segregated and further highlight the opposite spin sublattices (Mn_A and Mn_B) while c) shows the $C_2\mathbf{t}$ symmetry followed by a C_2 spin-space rotational symmetry between the opposite spin sublattices.

The pronounced distortion observed in $LaMnO_3$ (space group *Pbnm*) stems from the deformation of an ideal cubic perovskite due to the interplay of three primary factors. First, the pure shear distortion of the MnO_6 octahedra is attributed to the cooperative Jahn-Teller (JT) effect. This effect results in a coordinated shortening and elongation of the in-plane lattice vectors by $\bar{a} = a_0(x-y)$ and $\bar{b} = b_0(x+y)$, where terms $a_0 = b_0$ represent an ideal cubic perovskite's lattice parameters.[19] As a result, the O-Mn-O distances along an arbitrary bond direction will alternate (longer/shorter) for neighboring octahedra.[19] Second, $GdFeO_3$-type rotations (tilting) of the oxygen octahedra lead to a doubling of the unit cell along the c-axis. Finally, strain-induced displacements of La cations contribute to the overall orthorhombic

crystal classification.[19] Hund's rule and orbital ordering due to the cooperative Jahn-Teller effect induce local $S = 2$ spins on Mn^{3+} cations, which are ferromagnetically coupled in the *ab* plane and antiferromagnetically coupled along *c*, thus adopting the A-type magnetic ground state observed in experimental studies.[11,19,115,116] Spin splitting band diagrams for other isostructural perovskites, bearing A-type, C-type, and G-type magnetic grounds states, have also been calculated.[11,19]

The distorted $LaMnO_3$ crystal structure and its experimentally determined A-type magnetic ground state, depicted together in Figure 13a, begin to show familiar signatures of a suitable altermagnetic host. However, additional complexity distinguishes the coordination environment of this material from both the toy model and other altermagnetic candidates discussed in this review. In this case, each spin sublattice is comprised of four Mn octahedra in the *ab* plane of the unit cell, necessitating the transformation of all four Mn octahedra onto a layer with the opposite spin polarization. To visualize these symmetries, layers are segregated in Figure 13b. Seen in Figure 13c, the Mn_A sublattice transforms onto the Mn_B sublattice after a C_2 rotation around the crystallographic *b*-axis followed by a translation parallel to the [111] direction. The spin sublattice transforms, once again, by C_2. Taken together, the $[C_2||C_{2y}\mathbf{t}]$ nonrelativistic space group results in *d*-wave altermagnetic symmetry.[19]

$LaMnO_3$ is an insulator, and its proposed altermagnetic ground state cannot easily be demonstrated through the anomalous Hall effect (AHE) or by spectroscopic means, including the magneto-optical Kerr effect (MOKE), which shares the same symmetry requirements as the AHE.[102] This method requires magnetic field control of the spin structure.

Outlook

The publication of over three hundred papers on altermagnetism within the past two years is a reflection of the intense contemporary interest in this field.[117] So far, work on alter-

magnets has focused primarily on relatively simple crystalline materials that fit within the operational understanding of solid-state spintronic frameworks. Since the design principles or "ingredients" for altermagnetism are fairly straightforward: (1) a C_2 rotation that maps collinear spin-up and spin-down magnetic moments onto each other (therefore A- or G-type antiferromagnetic coupling) and (2) a rotation operator that acts only on the real space lattices associated with each spin center, there is tremendous opportunity for materials design/discovery of new altermagnets by chemists. Figure 14 highlights a selection of these research opportunities, which are discussed in greater detail below.

For relatively simple binary or ternary inorganic solids, the synthesis of crystalline phases under compression[118] could lead to the discovery of new altermagnetic materials in the composition–pressure–temperature phase space. Studies of cation-ordered perovskites[119] may now target specific tilting schemes that would have the requisite symmetry operations for altermagnetism. In intercalation compounds of transition metal dichalcogenides,[51,54,113] while stoichiometric considerations predominantly determine superlattice structure, a deeper understanding is needed for how intercalant and host choices dictate the nature of magnetic exchange (FM vs AFM) as well as the impact of synthetic conditions on disorder[120,121] and its ramifications on altermagnetic behavior.

As has proven to be the case for other magnetic materials, there are bound to be distinctive opportunities for organic or hybrid organic–inorganic compositions (including metal–organic frameworks) to produce altermagnetism and break current limits on the chemical programmability, tunability, and processability of altermagnetic materials.[122–124] The field of metal–organic magnets has made significant progress in developing magnetic platforms that incorporate molecular ligands, consist of abundant elements, exhibit ordering temperatures well above room temperature, and possess tunable coercivities.[123] A recent theoretical study has suggested that $M(\mathrm{pyz})_2$ where M = Ca or Sr, pyz = pyrazine, should possess an altermagnetic ground state.[125] Work on the compound κ–$(\mathrm{BEDT{-}TTF})_2\mathrm{Cu}[\mathrm{N(CN)_2}]X$ where X = Cl or Br (often abbreviated as κ–Cl or κ–Br, respectively),[12,126–128] highlights

that even molecular crystals and organic charge transfer salts can display altermagnetism. Still, the number of discovered/proposed organic or hybrid altermagnets remain limited. The use of ligand symmetry to dictate the rotational symmetry needed for altermagnetism could be fruitful. The design of porous frameworks in which rotational symmetry is induced by the adsorption of a molecule could enable the AHE to serve as a sensing readout in a conductive MOF.

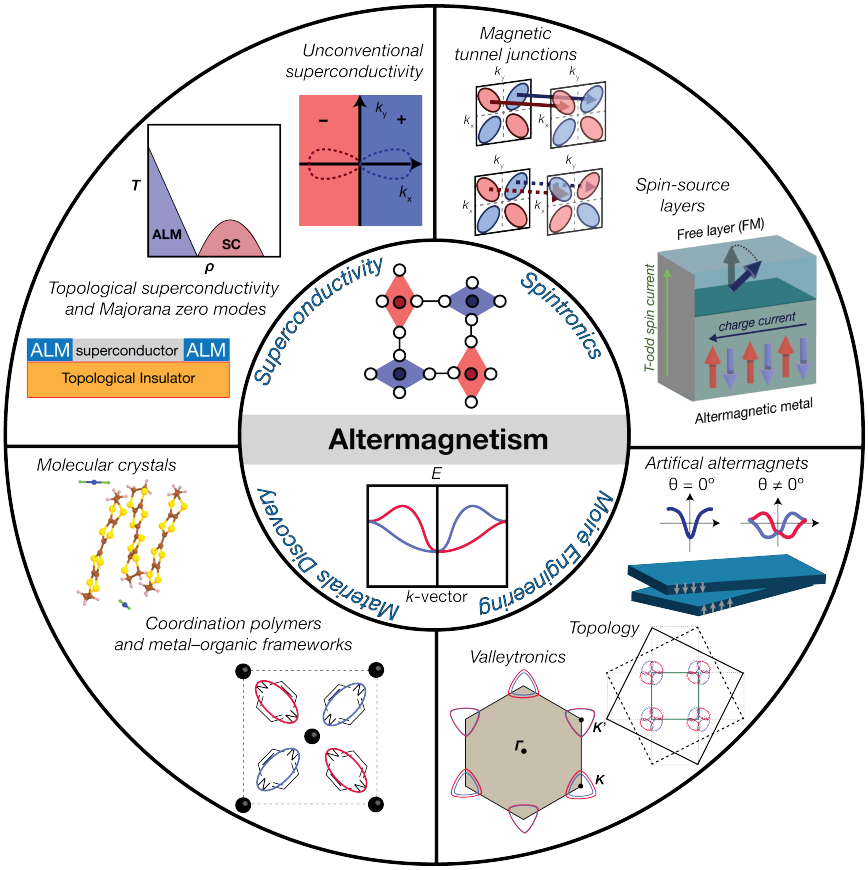

Figure 14: Opportunities for exploring and applying altermagnetism.

Since the isolation of graphene in 2004, 2D materials have garnered intense attention due to their wide range of physical properties, including long-range magnetic order.[129–132] Advances in probing and modulating the properties of 2D materials position dimensionality as another tool to investigate altermagnetism.[46,133–139] One interesting route is the synthesis of "artificial" altermagnets by assembly of 2D heterostructures in such a way that leads to the

emergence of spin–split bands. To realize non-relativistic spin-splitting in 2D crystals with interlayer AFM coupling (i.e., altermagnetism) requires that the two spin sublattices cannot be transposed by inversion, translation, planar mirror reflections, or their combinations. These individual symmetries and their combinations are, however, naturally broken by the introduction of an interlayer twist between the layers[133,134] This makes moiré engineering a route towards artificial altermagnets that are built from twisting conventional AFM crystals (provided the individual moments are aligned out of plane), and the magnitude of spin splitting would be twist tunable. Recent theoretical studies suggest that antiferromagnets, such as $MnPSe_3$ and FeTe, can host altermagnetism in twisted bilayer architectures, giving rise to spin–split bands despite the fact that the constituent monolayers are $\mathcal{PT}$–invariant.[133,134] It may also be worth investigating how moiré engineering can further augment the spin-splitting in 2D materials that are already proposed to be altermagnetic, such as RuF_4,,[46,137] and exploring electronic effects that arise due to the band folding and interlayer hybridization[140,141] of natively spin–split bands. Moiré engineering also enables the combination of altermagnetism and valleytronics (which involves exploiting the valley degree of freedom of a charge carrier)[142] as another conduit for realizing electrical manipulation of spins. The spin-polarized bands of ALMs are ordinarily valley degenerate. If artificial moiré ALMs are realized, it might be possible to use an out-of-plane electric field or uniaxial strain to generate a layer-dependent electrostatic potential that breaks valley degeneracy, enabling new opportunities for encoding and processing information in both the spin and valley degrees of freedom as long as equivalent valleys are near the Fermi level.[138,143]

The possible coexistence of altermagnetic and superconducting phases, along with novel properties that may arise when altermagnetic materials are placed in proximity to a superconductor, present intriguing avenues for exploration. While not experimentally verified, these are proposed routes to unconventional superconductivity.[12,144–147] In these cases, the spin fluctuations driven by altermagnetic order would be crucial for understanding possible Cooper pairing in altermagnets, by analogy to spin–triplet Cooper pairing induced by ferro-

magnetic order.[12,146–148] As in cuprates and other unconventional superconductors, the use of external stimuli, such as gating/doping and pressure, could provide control over superconductivity and magnetic order.[149,150] The connection in superconductivity between even- and odd-parity symmetry in momentum space may be approachable using altermagnets as it is proposed that $s-$, $p-$, and $d-$wave superconductivity can be achieved in altermagnets.[144,146,148,151] An interesting approach to interrogating the momentum–space features of altermagnets considers measuring the proximity effects between a superconductor and an altermagnet, where the orientation of momentum–split bands in the altermagnet can be manipulated by switching the direction of the Néel vector.[53,54,152] This strategy would provide an "on/off" switch where in the "on" state, the bands of the altermagnet are aligned with the superconductor, enabling Andreev reflection behavior.[89,153–159] Recent studies have also suggested that it might be possible to generate Majorana quasiparticles at the interface of a superconductor and altermagnet.[89,155,160,161] It is evident therefore that the potential coexistence of superconductivity and altermagnetism and related interfacial phenomena will likely provide a rich playground for the exploration of exotic physics.

Finally, a note on taxonomy: A notable limitation of the symmetry formalism discussed in recent works,[12,13] and within this perspective, is the exclusion of noncollinear spin-compensated structures and other AFM configurations that are known to exhibit NRSS phenomena.[21,162] Additionally, the contention that altermagnetism constitutes a "third magnetic phase" alongside ferromagnetism and antiferromagnetism (see Figure 1), remains an open question in the community. Some researchers question whether altermagnetism truly diverges from Louis Néel's definition of antiferromagnetism as an "antiparallel arrangement of atomic moments"– a definition that was later generalized to encompass both collinear and noncollinear magnetic order where the "sub-lattices exactly compensate".[163,164] Within this view, antiferromagnets and altermagnets in fact share a common foundational definition and altermagnetism would simply be a subset of antiferromagnetism. An alternative symmetry perspective offers a formalism that uses local spin-structure motifs, examining the local co-

ordination of magnetic moments to determine whether the geometries surrounding different spin alignments are interconvertible.[163] This formalism could help bridge the divide between collinear altermagnetism and related noncollinear AFMs exhibiting NRSS phenomena.

These considerations notwithstanding, the altermagnet concept offers well-defined principles that enable chemists and physicists to understand (and harness) NRSS phenomena in real material systems. In this Perspective, generalized for collinear spin configurations, we have sought to emphasize the key bonding symmetries, electronic phenomenology, and the practical potential of altermagnetic materials, while also illustrating their relationship to ferromagnets and "conventional" antiferromagnets.

Acknowledgement

We acknowledge helpful conversations with Lilia Xie and Matteo Michiardi. This material is based upon work supported by the US National Science Foundation, under award no. 2426144 (D.K.B). O.G. acknowledges support from the US National Science Foundation Graduate Research Fellowship Program for a predoctoral fellowship (grant no. DGE 1752814).

References

(1) Bhattacharya, P.; Fornari, R.; Kamimura, H. *Comprehensive Semiconductor Science and Technology*; Elsevier Science: Amsterdam London, 2011.

(2) Wolf, S. A.; Awschalom, D. D.; Buhrman, R. A.; Daughton, J. M.; Von Molnár, S.; Roukes, M. L.; Chtchelkanova, A. Y.; Treger, D. M. Spintronics: A Spin-Based Electronics Vision for the Future. *Science* **2001**, *294*, 1488–1495.

(3) Liao, Z.; Yamahara, H.; Terao, K.; Ma, K.; Seki, M.; Tabata, H. Short-term mem-

ory capacity analysis of $Lu_3Fe_4Co_{0.5}Si_{0.5}O_{12}$-based spin cluster glass towards reservoir computing. *Scientific Reports* **2023**, *13*, 5260.

(4) Pirro, P.; Vasyuchka, V. I.; Serga, A. A.; Hillebrands, B. Advances in coherent magnonics. *Nature Reviews Materials* **2021**, *6*, 1114–1135.

(5) Liu, Z. Noncollinear Antiferromagnetic Spintronics. *Materials Lab* **2022**, *1*.

(6) Jungwirth, T.; Marti, X.; Wadley, P.; Wunderlich, J. Antiferromagnetic spintronics. *Nature Nanotechnology* **2016**, *11*, 231–241.

(7) Deng, Y.; Liu, X.; Chen, Y.; Du, Z.; Jiang, N.; Shen, C.; Zhang, E.; Zheng, H.; Lu, H.-Z.; Wang, K. All-electrical switching of a topological non-collinear antiferromagnet at room temperature. *National Science Review* **2023**, *10*, nwac154.

(8) Wadley, P. et al. Electrical switching of an antiferromagnet. *Science* **2016**, *351*, 587–590.

(9) Tsai, H.; Higo, T.; Kondou, K.; Nomoto, T.; Sakai, A.; Kobayashi, A.; Nakano, T.; Yakushiji, K.; Arita, R.; Miwa, S.; Otani, Y.; Nakatsuji, S. Electrical manipulation of a topological antiferromagnetic state. *Nature* **2020**, *580*, 608–613.

(10) Nomoto, T.; Arita, R. Cluster multipole dynamics in noncollinear antiferromagnets. *Physical Review Research* **2020**, *2*, 012045.

(11) Yuan, L.-D.; Wang, Z.; Luo, J.-W.; Zunger, A. Prediction of low-Z collinear and noncollinear antiferromagnetic compounds having momentum-dependent spin splitting even without spin-orbit coupling. *Physical Review Materials* **2021**, *5*, 014409.

(12) Šmejkal, L.; Sinova, J.; Jungwirth, T. Emerging Research Landscape of Altermagnetism. *Physical Review X* **2022**, *12*, 040501.

(13) Šmejkal, L.; Sinova, J.; Jungwirth, T. Beyond Conventional Ferromagnetism and Antiferromagnetism: A Phase with Nonrelativistic Spin and Crystal Rotation Symmetry. *Physical Review X* **2022**, *12*, 031042.

(14) Wei, C.-C.; Lawrence, E.; Tran, A.; Ji, H. Crystal Chemistry and Design Principles of Altermagnets. *ACS Organic & Inorganic Au* **2024**, *4*, 604–619.

(15) Grzybowski, M. J.; Autieri, C.; Domagala, J.; Krasucki, C.; Kaleta, A.; Kret, S.; Gas, K.; Sawicki, M.; Bożek, R.; Suffczyński, J.; Pacuski, W. Wurtzite *vs.* rock-salt MnSe epitaxy: electronic and altermagnetic properties. *Nanoscale* **2024**, *16*, 6259–6267.

(16) Solovyev, I. V. Magneto-optical effect in the weak ferromagnets $LaMO_3$ (M = Cr, Mn, and Fe). *Phys. Rev. B* **1997**, *55*, 8060–8063.

(17) López-Moreno, S.; Romero, A. H.; Mejía-López, J.; Muñoz, A.; Roshchin, I. V. First-principles study of electronic, vibrational, elastic, and magnetic properties of FeF as a function of pressure. *Phys. Rev. B* **2012**, *85*, 134110.

(18) Noda, Y.; Ohno, K.; Nakamura, S. Momentum-dependent band spin splitting in semiconducting MnO_2 : a density functional calculation. *Phys. Chem. Chem. Phys.* **2016**, *18*, 13294–13303.

(19) Okugawa, T.; Ohno, K.; Noda, Y.; Nakamura, S. Weakly spin-dependent band structures of antiferromagnetic perovskite $LaMO_3$ (M = Cr, Mn, Fe). *Journal of Physics: Condensed Matter* **2018**, *30*, 075502.

(20) Landau, L. D.; Lifshits, E. M.; Pitaevskiĭ, L. P.; Landau, L. D. *Electrodynamics of Continuous Media*, 2nd ed.; Pergamon International Library of Science, Technology, Engineering, and Social Studies; Pergamon: Oxford; New York, 1984.

(21) Yuan, L.-D.; Georgescu, A. B.; Rondinelli, J. M. Non-relativistic spin splitting in compensated magnets that are not altermagnets. 2024-02-22. *arXiv (Condensed Matter, Materials Science)* arXiv:2402.14321, (accessed 2024-11-20).

(22) Yuan, L.-D.; Wang, Z.; Luo, J.-W.; Zunger, A. Strong influence of nonmagnetic ligands on the momentum-dependent spin splitting in antiferromagnets. *Physical Review B* **2021**, 224410.

(23) Hoffmann, R. How Chemistry and Physics Meet in the Solid State. *Angewandte Chemie International Edition in English* **1987**, *26*, 846–878.

(24) Tremel, W.; Hoffmann, R. Square nets of main-group elements in solid-state materials. *Journal of the American Chemical Society* **1987**, *109*, 124–140.

(25) Klemenz, S.; Lei, S.; Schoop, L. M. Topological Semimetals in Square-Net Materials. *Annual Review of Materials Research* **2019**, *49*, 185–206.

(26) Goesten, M. G.; Hoffmann, R. Mirrors of Bonding in Metal Halide Perovskites. *Journal of the American Chemical Society* **2018**, *140*, 12996–13010.

(27) Khoury, J. F.; Schoop, L. M. Chemical bonds in topological materials. *Trends in Chemistry* **2021**, *3*, 700–715.

(28) Burdett, J. K. From bonds to bands and molecules to solids. *Progress in Solid State Chemistry* **1984**, *15*, 173–255.

(29) Šmejkal, L.; González-Hernández, R.; Jungwirth, T.; Sinova, J. Crystal time-reversal symmetry breaking and spontaneous Hall effect in collinear antiferromagnets. *Science Advances* **2020**, *6*, eaaz8809.

(30) Šmejkal, L.; MacDonald, A. H.; Sinova, J.; Nakatsuji, S.; Jungwirth, T. Anomalous Hall antiferromagnets. *Nature Reviews Materials* **2022**, *7*, 482–496.

(31) Bai, L.; Feng, W.; Liu, S.; Šmejkal, L.; Mokrousov, Y.; Yao, Y. Altermagnetism: Exploring New Frontiers in Magnetism and Spintronics. *Advanced Functional Materials* **2024**, 2409327.

(32) Das, P.; Leeb, V.; Knolle, J.; Knap, M. Realizing Altermagnetism in Fermi-Hubbard Models with Ultracold Atoms. *Physical Review Letters* **2024**, *132*, 263402.

(33) Gomonay, O.; Kravchuk, V. P.; Jaeschke-Ubiergo, R.; Yershov, K. V.; Jungwirth, T.; Šmejkal, L.; Brink, J. V. D.; Sinova, J. Structure, control, and dynamics of altermagnetic textures. *npj Spintronics* **2024**, *2*, 35.

(34) Sattigeri, R. M.; Cuono, G.; Autieri, C. Altermagnetic surface states: towards the observation and utilization of altermagnetism in thin films, interfaces and topological materials. *Nanoscale* **2023**, *15*, 16998–17005.

(35) Sorantin, P. I.; Schwarz, K. Chemical bonding in rutile-type compounds. *Inorganic Chemistry* **1992**, *31*, 567–576.

(36) Bersuker, I. B. Jahn–Teller and Pseudo-Jahn–Teller Effects: From Particular Features to General Tools in Exploring Molecular and Solid State Properties. *Chemical Reviews* **2021**, *121*, 1463–1512.

(37) Mattheiss, L. F. Electronic structure of RuO_2, OsO_2, and IrO_2. *Physical Review B* **1976**, *13*, 2433–2450.

(38) Occhialini, C. A.; Bisogni, V.; You, H.; Barbour, A.; Jarrige, I.; Mitchell, J. F.; Comin, R.; Pelliciari, J. Local electronic structure of rutile RuO_2. *Physical Review Research* **2021**, *3*, 033214.

(39) Soumyanarayanan, A.; Reyren, N.; Fert, A.; Panagopoulos, C. Emergent phenomena induced by spin–orbit coupling at surfaces and interfaces. *Nature* **2016**, *539*, 509–517.

(40) Rashba, E. Properties of semiconductors with an extremum loop. I. Cyclotron and combinational Resonance in a magnetic field perpendicular to the plane of the loop. *Sov. Phys.-Solid State* **1960**, *2*, 1109.

(41) Feng, Y. et al. Rashba-like spin splitting along three momentum directions in trigonal layered PtBi2. *Nature Communications* **2019**, *10*, 4765.

(42) Maurer, B.; Vorwerk, C.; Draxl, C. Rashba and Dresselhaus effects in two-dimensional Pb-I-based perovskites. *Physical Review B* **2022**, *105*, 155149.

(43) Meier, L.; Salis, G.; Shorubalko, I.; Gini, E.; Schön, S.; Ensslin, K. Measurement of Rashba and Dresselhaus spin–orbit magnetic fields. *Nature Physics* **2007**, *3*, 650–654.

(44) Krempaský, J. et al. Altermagnetic lifting of Kramers spin degeneracy. *Nature* **2024**, *626*, 517–522.

(45) Kluczyk, K. P.; Gas, K.; Grzybowski, M. J.; Skupiński, P.; Borysiewicz, M. A.; Fas, T.; Suffczyński, J.; Domagala, J. Z.; Grasza, K.; Mycielski, A.; Baj, M.; Ahn, K. H.; Výborný, K.; Sawicki, M.; Gryglas-Borysiewicz, M. Coexistence of anomalous Hall effect and weak magnetization in a nominally collinear antiferromagnet MnTe. *Physical Review B* **2024**, *110*, 155201.

(46) Milivojević, M.; Orozović, M.; Picozzi, S.; Gmitra, M.; Stavrić, S. Interplay of altermagnetism and weak ferromagnetism in two-dimensional RuF_4. *2D Materials* **2024**, *11*, 035025.

(47) Nagaosa, N.; Sinova, J.; Onoda, S.; MacDonald, A. H.; Ong, N. P. Anomalous Hall effect. *Reviews of Modern Physics* **2010**, *82*, 1539–1592.

(48) Chen, H.; Niu, Q.; MacDonald, A. Anomalous Hall Effect Arising from Noncollinear Antiferromagnetism. *Physical Review Letters* **2014**, *112*, 017205.

(49) Koizumi, H.; Yamasaki, Y.; Yanagihara, H. Quadrupole anomalous Hall effect in magnetically induced electron nematic state. *Nature Communications* **2023**, *14*, 8074.

(50) Du, K.; Xu, X.; Won, C.; Wang, K.; Crooker, S. A.; Rangan, S.; Bartynski, R.; Cheong, S.-W. Topological surface magnetism and Néel vector control in a magnetoelectric antiferromagnet. *npj Quantum Materials* **2023**, *8*, 17.

(51) Xie, L. S.; Husremović, S.; Gonzalez, O.; Craig, I. M.; Bediako, D. K. Structure and Magnetism of Iron- and Chromium-Intercalated Niobium and Tantalum Disulfides. *Journal of the American Chemical Society* **2022**, *144*, 9525–9542.

(52) Nye, J. F. *Physical properties of crystals: their representation by tensors and matrices*, reprinted ed.; Oxford science publications; Clarendon Press: Oxford, 2012.

(53) Smolyanyuk, A.; Šmejkal, L.; Mazin, I. I. A tool to check whether a symmetry-compensated collinear magnetic material is antiferro- or altermagnetic. *SciPost Physics Codebases* **2024**, 30.

(54) Regmi, R. B. et al. Altermagnetism in the layered intercalated transition metal dichalcogenide $CoNb_4Se_8$. 2024-08-16. *arXiv (Condensed Matter, Strongly Correlated Electrons)* arXiv:2408.08835, (accessed 2024-11-20).

(55) Berry, V., Michael Quantal phase factors accompanying adiabatic changes. *Proceedings of the Royal Society of London. A. Mathematical and Physical Sciences* **1984**, *392*, 45–57.

(56) Pancharatnam, S. Generalized theory of interference, and its applications: Part I. Coherent pencils. *Proceedings of the Indian Academy of Sciences - Section A* **1956**, *44*, 247–262.

(57) Oprea, J. Geometry and the Foucault Pendulum. *The American Mathematical Monthly* **1995**, *102*, 515–522.

(58) Golin, S.; Knauf, A.; Marmi, S. The Hannay angles: Geometry, adiabaticity, and an example. *Communications In Mathematical Physics* **1989**, *123*, 95–122.

(59) Aharonov, Y.; Bohm, D. Significance of Electromagnetic Potentials in the Quantum Theory. *Physical Review* **1959**, *115*, 485–491.

(60) Longuet-Higgins, C., Hugh; Opik, U.; Pryce, M.; Sack, A., R. Studies of the Jahn-Teller effect .II. The dynamical problem. *Proceedings of the Royal Society of London. Series A. Mathematical and Physical Sciences* **1958**, *244*, 1–16.

(61) Herzberg, G.; Longuet-Higgins, H. C. Intersection of potential energy surfaces in polyatomic molecules. *Discussions of the Faraday Society* **1963**, *35*, 77.

(62) Thouless, D.; Ao, P.; Niu, Q. Vortex dynamics in superfluids and the Berry phase. *Physica A: Statistical Mechanics and its Applications* **1993**, *200*, 42–49.

(63) Xiao, D.; Chang, M.-C.; Niu, Q. Berry phase effects on electronic properties. *Reviews of Modern Physics* **2010**, *82*, 1959–2007.

(64) Bruno, P. Berry phase effects in magnetism. 2005-06-13. *arXiv (Condensed Matter, Mesoscale and Nanoscale Physics)* arXiv:cond–mat/0506270, (accessed 2024-11-20).

(65) Yan, B.; Felser, C. Topological Materials: Weyl Semimetals. *Annual Review of Condensed Matter Physics* **2017**, *8*, 337–354.

(66) Sato, T.; Haddad, S.; Fulga, I. C.; Assaad, F. F.; Van Den Brink, J. Altermagnetic Anomalous Hall Effect Emerging from Electronic Correlations. *Physical Review Letters* **2024**, *133*, 086503.

(67) Bhatti, S.; Sbiaa, R.; Hirohata, A.; Ohno, H.; Fukami, S.; Piramanayagam, S. Spintronics based random access memory: a review. *Materials Today* **2017**, *20*, 530–548.

(68) Heindl, R.; Rippard, W. H.; Russek, S. E.; Pufall, M. R. Time-domain analysis of spin-torque induced switching paths in nanoscale CoFeB/MgO/CoFeB magnetic tunnel junction devices. *Journal of Applied Physics* **2014**, *116*, 243902.

(69) Evarts, E. R.; Heindl, R.; Rippard, W. H.; Pufall, M. R. Correlation of anomalous write error rates and ferromagnetic resonance spectrum in spin-transfer-torque-magnetic-random-access-memory devices containing in-plane free layers. *Applied Physics Letters* **2014**, *104*, 212402.

(70) Engel, B.; Akerman, J.; Butcher, B.; Dave, R.; DeHerrera, M.; Durlam, M.; Grynkewich, G.; Janesky, J.; Pietambaram, S.; Rizzo, N.; Slaughter, J.; Smith, K.; Sun, J.; Tehrani, S. A 4-Mb toggle MRAM based on a novel bit and switching method. *IEEE Transactions on Magnetics* **2005**, *41*, 132–136.

(71) Chappert, C.; Fert, A.; Van Dau, F. N. The emergence of spin electronics in data storage. *Nature Materials* **2007**, *6*, 813–823.

(72) Slonczewski, J. Current-driven excitation of magnetic multilayers. *Journal of Magnetism and Magnetic Materials* **1996**, *159*, L1–L7.

(73) Berger, L. Emission of spin waves by a magnetic multilayer traversed by a current. *Physical Review B* **1996**, *54*, 9353–9358.

(74) Albert, F. J.; Katine, J. A.; Buhrman, R. A.; Ralph, D. C. Spin-polarized current switching of a Co thin film nanomagnet. *Applied Physics Letters* **2000**, *77*, 3809–3811.

(75) Kim, K.-W.; Park, B.-G.; Lee, K.-J. Spin current and spin-orbit torque induced by ferromagnets. *npj Spintronics* **2024**, *2*, 8.

(76) Mihai Miron, I.; Gaudin, G.; Auffret, S.; Rodmacq, B.; Schuhl, A.; Pizzini, S.; Vo-

gel, J.; Gambardella, P. Current-driven spin torque induced by the Rashba effect in a ferromagnetic metal layer. *Nature Materials* **2010**, *9*, 230–234.

(77) Liu, L.; Pai, C.-F.; Li, Y.; Tseng, H. W.; Ralph, D. C.; Buhrman, R. A. Spin-Torque Switching with the Giant Spin Hall Effect of Tantalum. *Science* **2012**, *336*, 555–558.

(78) Manchon, A.; Železný, J.; Miron, I.; Jungwirth, T.; Sinova, J.; Thiaville, A.; Garello, K.; Gambardella, P. Current-induced spin-orbit torques in ferromagnetic and antiferromagnetic systems. *Reviews of Modern Physics* **2019**, *91*, 035004.

(79) Ryu, J.; Lee, S.; Lee, K.; Park, B. Current-Induced Spin–Orbit Torques for Spintronic Applications. *Advanced Materials* **2020**, *32*, 1907148.

(80) Jungwirth, T.; Wunderlich, J.; Olejník, K. Spin Hall effect devices. *Nature Materials* **2012**, *11*, 382–390.

(81) Edelstein, V. Spin polarization of conduction electrons induced by electric current in two-dimensional asymmetric electron systems. *Solid State Communications* **1990**, *73*, 233–235.

(82) Ganichev, S. D.; Ivchenko, E. L.; Bel'kov, V. V.; Tarasenko, S. A.; Sollinger, M.; Weiss, D.; Wegscheider, W.; Prettl, W. Spin-galvanic effect. *Nature* **2002**, *417*, 153–156.

(83) González-Hernández, R.; Šmejkal, L.; Výborný, K.; Yahagi, Y.; Sinova, J.; Jungwirth, T.; Železný, J. Efficient Electrical Spin Splitter Based on Nonrelativistic Collinear Antiferromagnetism. *Physical Review Letters* **2021**, *126*, 127701.

(84) Karube, S.; Tanaka, T.; Sugawara, D.; Kadoguchi, N.; Kohda, M.; Nitta, J. Observation of Spin-Splitter Torque in Collinear Antiferromagnetic RuO_2. *Physical Review Letters* **2022**, *129*, 137201.

(85) Shao, D.-F.; Tsymbal, E. Y. Antiferromagnetic tunnel junctions for spintronics. *npj Spintronics* **2024**, *2*, 13.

(86) Rimmler, B. H.; Pal, B.; Parkin, S. S. P. Non-collinear antiferromagnetic spintronics. *Nature Reviews Materials* **2024**, 1.

(87) Nair, N. L.; Maniv, E.; John, C.; Doyle, S.; Orenstein, J.; Analytis, J. G. Electrical switching in a magnetically intercalated transition metal dichalcogenide. *Nature Materials* **2020**, *19*, 153–157.

(88) Bodnar, S. Y.; Šmejkal, L.; Turek, I.; Jungwirth, T.; Gomonay, O.; Sinova, J.; Sapozhnik, A. A.; Elmers, H.-J.; Kläui, M.; Jourdan, M. Writing and reading antiferromagnetic Mn_2Au by Néel spin-orbit torques and large anisotropic magnetoresistance. *Nature Communications* **2018**, *9*, 348.

(89) Giil, H. G.; Linder, J. Superconductor-altermagnet memory functionality without stray fields. *Physical Review B* **2024**, *109*, 134511.

(90) Berlijn, T.; Snijders, P.; Delaire, O.; Zhou, H.-D.; Maier, T.; Cao, H.-B.; Chi, S.-X.; Matsuda, M.; Wang, Y.; Koehler, M.; Kent, P.; Weitering, H. Itinerant Antiferromagnetism in RuO_2. *Physical Review Letters* **2017**, *118*, 077201.

(91) Feng, Z. et al. An anomalous Hall effect in altermagnetic ruthenium dioxide. *Nature Electronics* **2022**, *5*, 735–743.

(92) Hiraishi, M.; Okabe, H.; Koda, A.; Kadono, R.; Muroi, T.; Hirai, D.; Hiroi, Z. Nonmagnetic Ground State in RuO_2 Revealed by Muon Spin Rotation. *Physical Review Letters* **2024**, *132*, 166702.

(93) Kiefer, L.; Wirth, F.; Bertin, A.; Becker, P.; Bohatý, L.; Schmalzl, K.; Stunault, A.; Rodríguez-Velamazán, J. A.; Fabelo, O.; Braden, M. Crystal structure and absence

of magnetic order in single crystalline RuO_2. 2024-10-8. *arXiv (Condensed Matter, Materials Science)* arXiv:2410.05850, (accessed 2024-11-20).

(94) Liu, J. et al. Absence of Altermagnetic Spin Splitting Character in Rutile Oxide RuO_2. *Physical Review Letters* **2024**, *133*, 176401.

(95) Bossini, D.; Terschanski, M.; Mertens, F.; Springholz, G.; Bonanni, A.; Uhrig, G. S.; Cinchetti, M. Exchange-mediated magnetic blue-shift of the band-gap energy in the antiferromagnetic semiconductor MnTe. *New Journal of Physics* **2020**, *22*, 083029.

(96) Collaboration: Authors and editors of the volumes III/17G-41D In *Non-Tetrahedrally Bonded Binary Compounds II*; Madelung, O., Rössler, U., Schulz, M., Eds.; Springer-Verlag: Berlin/Heidelberg, 2000; Vol. 41D; pp 1–3, Series Title: Landolt-Börnstein - Group III Condensed Matter.

(97) Kunitomi, N.; Hamaguchi, Y.; Anzai, S. Neutron diffraction study on manganese telluride. *Journal de Physique* **1964**, *25*, 568–574.

(98) Szuszkiewicz, W.; Hennion, B.; Witkowska, B.; Łusakowska, E.; Mycielski, A. Neutron scattering study of structural and magnetic properties of hexagonal MnTe. *physica status solidi (c)* **2005**, *2*, 1141–1146.

(99) Komatsubara, T.; Murakami, M.; Hirahara, E. Magnetic Properties of Manganese Telluride Single Crystals. *Journal of the Physical Society of Japan* **1963**, *18*, 356–364.

(100) Sobota, J. A.; He, Y.; Shen, Z.-X. Angle-resolved photoemission studies of quantum materials. *Reviews of Modern Physics* **2021**, *93*, 025006.

(101) Lin, C.-Y.; Moreschini, L.; Lanzara, A. Present and future trends in spin ARPES. *Europhysics Letters* **2021**, *134*, 57001.

(102) Mazin, I. I. Altermagnetism in MnTe: Origin, predicted manifestations, and routes to detwinning. *Physical Review B* **2023**, *107*, L100418.

(103) Kriegner, D.; Výborný, K.; Olejník, K.; Reichlová, H.; Novák, V.; Marti, X.; Gazquez, J.; Saidl, V.; Němec, P.; Volobuev, V. V.; Springholz, G.; Holý, V.; Jungwirth, T. Multiple-stable anisotropic magnetoresistance memory in antiferromagnetic MnTe. *Nature Communications* **2016**, *7*, 11623.

(104) Marti, X. et al. Room-temperature antiferromagnetic memory resistor. *Nature Materials* **2014**, *13*, 367–374.

(105) Osumi, T.; Souma, S.; Aoyama, T.; Yamauchi, K.; Honma, A.; Nakayama, K.; Takahashi, T.; Ohgushi, K.; Sato, T. Observation of a giant band splitting in altermagnetic MnTe. *Physical Review B* **2024**, *109*, 115102.

(106) Higo, T. et al. Large magneto-optical Kerr effect and imaging of magnetic octupole domains in an antiferromagnetic metal. *Nature Photonics* **2018**, *12*, 73–78.

(107) Šmejkal, L.; Hellenes, A. B.; González-Hernández, R.; Sinova, J.; Jungwirth, T. Giant and Tunneling Magnetoresistance in Unconventional Collinear Antiferromagnets with Nonrelativistic Spin-Momentum Coupling. *Physical Review X* **2022**, *12*, 011028.

(108) Gonzalez Betancourt, R.; Zubáč, J.; Gonzalez-Hernandez, R.; Geishendorf, K.; Šobáň, Z.; Springholz, G.; Olejník, K.; Šmejkal, L.; Sinova, J.; Jungwirth, T.; Goennenwein, S.; Thomas, A.; Reichlová, H.; Železný, J.; Kriegner, D. Spontaneous Anomalous Hall Effect Arising from an Unconventional Compensated Magnetic Phase in a Semiconductor. *Physical Review Letters* **2023**, *130*, 036702.

(109) Dal Din, A.; Amin, O. J.; Wadley, P.; Edmonds, K. W. Antiferromagnetic spintronics and beyond. *npj Spintronics* **2024**, *2*, 25.

(110) Hall, A. E.; Khalyavin, D. D.; Manuel, P.; Mayoh, D. A.; Orlandi, F.; Petrenko, O. A.; Lees, M. R.; Balakrishnan, G. Magnetic structure investigation of the intercalated transition metal dichalcogenide $V_{1/3}NbS_2$. *Physical Review B* **2021**, *103*, 174431.

(111) Lu, K.; Sapkota, D.; DeBeer-Schmitt, L.; Wu, Y.; Cao, H. B.; Mannella, N.; Mandrus, D.; Aczel, A. A.; MacDougall, G. J. Canted antiferromagnetic order in the monoaxial chiral magnets $V_{1/3}TaS_2$ and $V_{1/3}NbS_2$. *Physical Review Materials* **2020**, *4*, 054416.

(112) Lawrence, E. A. et al. Fe Site Order and Magnetic Properties of $Fe_{1/4}NbS_2$. *Inorganic Chemistry* **2023**, *62*, 18179–18188.

(113) Mandujano, H. C.; Salas, G. S.; Li, T.; Zavalij, P. Y.; Manjón-Sanz, A.; Butch, N. P.; Rodriguez, E. E. Itinerant *A*-type antiferromagnetic order in $Co_{1/4}TaSe_2$. *Phys. Rev. B* **2024**, *110*, 144420.

(114) Bernardini, F.; Fiebig, M.; Cano, A. Ruddlesden-Popper and perovskite phases as a material platform for altermagnetism. 2024-01-23. *arXiv (Condensed Matter, Materials Science)* arXiv:2401.12910, (accessed 2024-11-20).

(115) Pavarini, E.; Koch, E. Origin of Jahn-Teller Distortion and Orbital Order in $LaMnO_3$. *Physical Review Letters* **2010**, *104*, 086402.

(116) Koehler, W.; Wollan, E. Neutron-diffraction study of the magnetic properties of perovskite-like compounds $LaBO_3$. *Journal of Physics and Chemistry of Solids* **1957**, *2*, 100–106.

(117) Jungwirth, T.; Fernandes, R. M.; Sinova, J.; Smejkal, L. Altermagnets and beyond: Nodal magnetically-ordered phases. 2024-09-16. *arXiv (Condensed Matter, Materials Science)* arXiv:2409.10034, (accessed 2024-11-20).

(118) Walsh, J. P. S.; Freedman, D. E. High-Pressure Synthesis: A New Frontier in the Search for Next-Generation Intermetallic Compounds. *Accounts of Chemical Research* **2018**, *51*, 1315–1323.

(119) King, G.; Woodward, P. M. Cation ordering in perovskites. *J. Mater. Chem.* **2010**, *20*, 5785–5796.

(120) Choe, J.; Lee, K.; Huang, C.-L.; Trivedi, N.; Morosan, E. Magnetotransport in Fe-intercalated TS$_2$: Comparison between T = Ti and Ta. *Phys. Rev. B* **2019**, *99*, 064420.

(121) Goodge, B. H.; Gonzalez, O.; Xie, L. S.; Bediako, D. K. Consequences and Control of Multiscale Order/Disorder in Chiral Magnetic Textures. *ACS Nano* **2023**, *17*, 19865–19876.

(122) Thorarinsdottir, A. E.; Harris, T. D. Metal–Organic Framework Magnets. *Chemical Reviews* **2020**, *120*, 8716–8789.

(123) Perlepe, P. et al. Metal-organic magnets with large coercivity and ordering temperatures up to 242°C. *Science* **2020**, *370*, 587–592.

(124) Coronado, E. Molecular magnetism: from chemical design to spin control in molecules, materials and devices. *Nature Reviews Materials* **2019**, *5*, 87–104.

(125) Che, Y.; Lv, H.; Wu, X.; Yang, J. Realizing altermagnetism in two-dimensional metal–organic framework semiconductors with electric-field-controlled anisotropic spin current. *Chemical Science* **2024**, *15*, 13853–13863.

(126) Naka, M.; Hayami, S.; Kusunose, H.; Yanagi, Y.; Motome, Y.; Seo, H. Anomalous Hall effect in -type organic antiferromagnets. *Physical Review B* **2020**, *102*, 075112.

(127) Iguchi, S.; Kobayashi, H.; Ikemoto, Y.; Furukawa, T.; Itoh, H.; Iwai, S.; Moriwaki, T.; Sasaki, T. Magneto-optical Detection of Altermagnetism in Organic Antiferromagnet. 2024-09-24. *arXiv (Condensed Matter, Strongly Correlated Electrons)* arXiv:2409.15696, (accessed 2024-11-20).

(128) Naka, M.; Hayami, S.; Kusunose, H.; Yanagi, Y.; Motome, Y.; Seo, H. Spin current generation in organic antiferromagnets. *Nature Communications* **2019**, *10*, 4305.

(129) Zeng, M.; Xiao, Y.; Liu, J.; Yang, K.; Fu, L. Exploring Two-Dimensional Materials toward the Next-Generation Circuits: From Monomer Design to Assembly Control. *Chemical Reviews* **2018**, *118*, 6236–6296.

(130) Lei, Y. et al. Graphene and Beyond: Recent Advances in Two-Dimensional Materials Synthesis, Properties, and Devices. *ACS Nanoscience Au* **2022**, *2*, 450–485.

(131) Wang, Q. H. et al. The Magnetic Genome of Two-Dimensional van der Waals Materials. *ACS Nano* **2022**, *16*, 6960–7079.

(132) Gibertini, M.; Koperski, M.; Morpurgo, A. F.; Novoselov, K. S. Magnetic 2D materials and heterostructures. *Nature Nanotechnology* **2019**, *14*, 408–419.

(133) Liu, Y.; Yu, J.; Liu, C.-C. Twisted Magnetic Van der Waals Bilayers: An Ideal Platform for Altermagnetism. *Physical Review Letters* **2024**, *133*, 206702.

(134) Sheoran, S.; Bhattacharya, S. Nonrelativistic spin splittings and altermagnetism in twisted bilayers of centrosymmetric antiferromagnets. *Physical Review Materials* **2024**, *8*, L051401.

(135) Liu, Q.; Kang, J.; Wang, P.; Gao, W.; Qi, Y.; Zhao, J.; Jiang, X. Inverse Magnetocaloric Effect in Altermagnetic 2D Non-van der Waals FeX (X = S and Se) Semiconductors. *Advanced Functional Materials* **2024**, *34*, 2402080.

(136) González, J. W.; León, A. M.; González-Fuentes, C.; Gallardo, R. A. Altermagnetism in Two Dimensional Ca-Ru-O Perovskite. 2024-08-16. *arXiv (Condensed Matter, Materials Science)* arXiv:2408.08999, (accessed 2024-11-20).

(137) Sødequist, J.; Olsen, T. Two-dimensional altermagnets from high throughput computational screening: Symmetry requirements, chiral magnons, and spin-orbit effects. *Applied Physics Letters* **2024**, *124*, 182409.

(138) Wu, Y.; Deng, L.; Yin, X.; Tong, J.; Tian, F.; Zhang, X. Valley-Related Multipiezo Effect and Noncollinear Spin Current in an Altermagnet Fe_2Se_2O Monolayer. *Nano Letters* **2024**, *24*, 10534–10539.

(139) Zeng, S.; Zhao, Y.-J. Description of two-dimensional altermagnetism: Categorization using spin group theory. *Physical Review B* **2024**, *110*, 054406.

(140) Yang, K.; Liu, Y.; Schindler, F.; Liu, C.-X. Engineering Miniband Topology via Band-Folding in Moiré Superlattice Materials. 2024-05-21. *arXiv (Condensed Matter, Mesoscale and Nanoscale Physics)* arXiv:2405.13145, (accessed 2024-11-20).

(141) Bistritzer, R.; MacDonald, A. H. Moiré bands in twisted double-layer graphene. *Proceedings of the National Academy of Sciences* **2011**, *108*, 12233–12237.

(142) Schaibley, J. R.; Yu, H.; Clark, G.; Rivera, P.; Ross, J. S.; Seyler, K. L.; Yao, W.; Xu, X. Valleytronics in 2D materials. *Nature Reviews Materials* **2016**, *1*, 16055.

(143) Guo, S.-D.; Liu, Y.; Liu, C.-C. Valley polarization in twisted altermagnetism. 2024-06-20. *arXiv (Condensed Matter, Materials Science)* arXiv:2406.13950, (accessed 2024-11-20).

(144) Zhu, D.; Zhuang, Z.-Y.; Wu, Z.; Yan, Z. Topological superconductivity in two-dimensional altermagnetic metals. *Physical Review B* **2023**, *108*, 184505.

(145) Chakraborty, D.; Black-Schaffer, A. M. Zero-field finite-momentum and field-induced superconductivity in altermagnets. *Physical Review B* **2024**, *110*, L060508.

(146) Bose, A.; Vadnais, S.; Paramekanti, A. Altermagnetism and superconductivity in a

multiorbital t-J model. 2024-03-25. *arXiv (Condensed Matter, Strongly Correlated Electrons)* arXiv:2403.17050, (accessed 2024-11-20).

(147) Chakraborty, D.; Black-Schaffer, A. M. Constraints on superconducting pairing in altermagnets. 2024-08-7. *arXiv (Condensed Matter, Superconductivity)* arXiv:2408.03999, (accessed 2024-11-20).

(148) Mazin, I. I. Notes on altermagnetism and superconductivity. 2022-03-9. *arXiv (Condensed Matter, Superconductivity)* arXiv:2203.05000, (accessed 2024-11-20).

(149) Scalapino, D. J. A common thread: The pairing interaction for unconventional superconductors. *Reviews of Modern Physics* **2012**, *84*, 1383–1417.

(150) Norman, M. R. The Challenge of Unconventional Superconductivity. *Science* **2011**, *332*, 196–200.

(151) Brekke, B.; Brataas, A.; Sudbø, A. Two-dimensional altermagnets: Superconductivity in a minimal microscopic model. *Physical Review B* **2023**, *108*, 224421.

(152) Banerjee, S.; Scheurer, M. S. Altermagnetic superconducting diode effect. *Physical Review B* **2024**, *110*, 024503.

(153) Zhang, S.-B.; Hu, L.-H.; Neupert, T. Finite-momentum Cooper pairing in proximitized altermagnets. *Nature Communications* **2024**, *15*, 1801.

(154) Sun, C.; Brataas, A.; Linder, J. Andreev reflection in altermagnets. *Physical Review B* **2023**, *108*, 054511.

(155) Papaj, M. Andreev reflection at the altermagnet-superconductor interface. *Physical Review B* **2023**, *108*, L060508.

(156) Ouassou, J. A.; Brataas, A.; Linder, J. dc Josephson Effect in Altermagnets. *Physical Review Letters* **2023**, *131*, 076003.

(157) Chourasia, S.; Svetogorov, A.; Kamra, A.; Belzig, W. Thermodynamic properties of a superconductor interfaced with an altermagnet. 2024-03-15. *arXiv (Condensed Matter, Superconductivity)* arXiv:2403.10456, (accessed 2024-11-20).

(158) Kazmin, D.; Esin, V.; Barash, Y.; Timonina, A.; Kolesnikov, N.; Deviatov, E. Andreev reflection for MnTe altermagnet candidate. *Physica B: Condensed Matter* **2025**, *696*, 416602.

(159) Niu, Z. P.; Yang, Z. Orientation-dependent Andreev reflection in an altermagnet/altermagnet/superconductor junction. *Journal of Physics D: Applied Physics* **2024**, *57*, 395301.

(160) Li, Y.-X.; Liu, C.-C. Majorana corner modes and tunable patterns in an altermagnet heterostructure. *Physical Review B* **2023**, *108*, 205410.

(161) Ghorashi, S. A. A.; Hughes, T. L.; Cano, J. Altermagnetic Routes to Majorana Modes in Zero Net Magnetization. 2023-06-15. *arXiv (Condensed Matter, Mesoscale and Nanoscale Physics)* arXiv:2306.09413, (accessed 2024-11-20).

(162) Yuan, L.-D.; Zhang, X.; Acosta, C. M.; Zunger, A. Uncovering spin-orbit coupling-independent hidden spin polarization of energy bands in antiferromagnets. *Nature Communications* **2023**, *14*, 5301.

(163) Yuan, L.; Zunger, A. Degeneracy Removal of Spin Bands in Collinear Antiferromagnets with Non-Interconvertible Spin-Structure Motif Pair. *Advanced Materials* **2023**, *35*, 2211966.

(164) Néel, L. Antiferromagnetism and Ferrimagnetism. *Proceedings of the Physical Society. Section A* **1952**, *65*, 869–885.

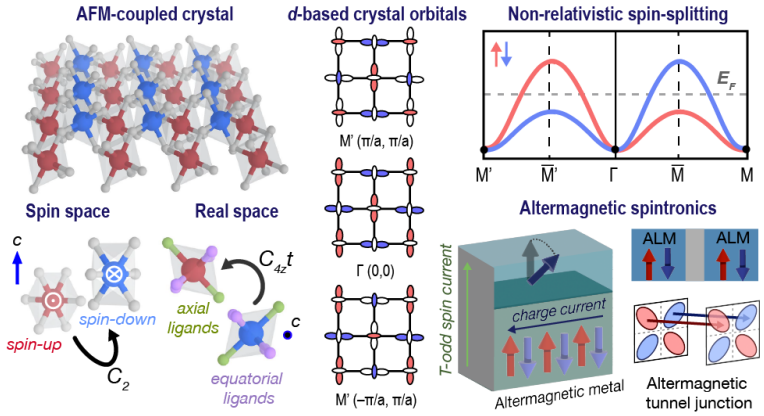

Table of Contents graphic